Group Identification and Variable Selection in Multivariable Mendelian Randomization with Highly-Correlated Exposures

Yinxiang Wu¹, Neil M. Davies^{2,3,4}, Ting Ye¹

- ¹Department of Biostatistics, University of Washington, Seattle, Washington, U.S.A.
 - ² Division of Psychiatry, University College London, London WC1E 6BT, UK.
- ³ Department of Statistical Science, University College London, London WC1E 6BT, UK.
- ⁴ Department of Public Health and Nursing, Norwegian University of Science and Technology, Norway.

Abstract

Multivariable Mendelian Randomization (MVMR) estimates the direct causal effects of multiple risk factors on an outcome using genetic variants as instruments. The growing availability of summary-level genetic data has created opportunities to apply MVMR in high-dimensional settings with many strongly correlated candidate risk factors. However, existing methods face three major limitations: weak instrument bias, limited interpretability, and the absence of valid post-selection inference. Here we introduce MVMR-PACS, a method that identifies signal-groups—sets of causal risk factors with high genetic correlation or indistinguishable causal effects—and estimates the direct effect of each group. MVMR-PACS minimizes a debiased objective function that reduces weak instrument bias while yielding interpretable estimates with theoretical guarantees for variable selection. We adapt a data-thinning strategy to summary-data MVMR to enable valid post-selection inference. In simulations, MVMR-PACS outperforms existing approaches in both estimation accuracy and variable selection. When applied to 27 lipoprotein subfraction traits and coronary artery disease risk, MVMR-PACS identifies biologically meaningful and robust signal-groups with interpretable direct causal effects.

Keywords: Causal Inference; GWAS; Variable Selection; Post-selection Inference; Weak Instruments

1 Introduction

Multivariable Mendelian randomization (MVMR) uses genetic variants as instrumental variables to estimate the direct causal effects of multiple exposures on an outcome [1, 2]. With the growing availability of summary-level genetic association data, summary-data MVMR has been widely applied across various fields [3, 4], including causal inference with omics data [5–7]. However, as the number and correlation of exposures increase, current MVMR methods face three critical challenges that limit their reliability: weak instrument bias arising from highly correlated exposures, difficulty in selecting true causal factors or interpretable groups among many candidates, and lack of valid post-selection inference. Addressing these challenges is essential for extending MVMR to modern high-dimensional omics applications, which often involve many highly correlated exposures.

MVMR requires genetic variants (typically single-nucleotide polymorphisms, or SNPs) to satisfy three core assumptions [8, 9] (Figure 1a):

- i *Relevance*: SNPs must be strongly associated with each exposure, conditional on the other exposures in the model;
- ii *Independence*: SNPs are independent of all confounders of the exposures and outcome;
- iii Exclusion restriction: SNPs affect the outcome only through the included exposures.

Unlike univariable MR, which assumes genetic instruments affect the outcome through a single exposure, MVMR incorporates multiple exposures to strengthen the plausibility of the exclusion restriction by adjusting for known pleiotropic pathways. However, this adjustment creates a fundamental trade-off: when exposures are correlated, conditioning on multiple exposures weakens the conditional associations between SNPs and individual exposures. Even when SNPs show strong marginal associations with each exposure—indicating strong instruments in a univariable setting—their conditional associations can become weak when genetic effects on different exposures are highly correlated [9–11]. This problem is particularly acute in omics applications, where genetic correlations between molecular traits such as metabolites or proteins often exceed 0.8 [12–14]. In these

cases, standard estimators such as MVMR-IVW [15], MVMR-Egger [16], and MVMR-Median [17], as well as recent weak-instrument-robust methods including GRAPPLE [18], MVMR-cML [19], MRBEE [20], and SRIVW [11], can yield biased, imprecise, or unstable estimates. Consequently, practitioners often avoid MVMR entirely, opting instead for extensive univariable MR analyses or restricting MVMR to a few preselected exposures—approaches that impose heavy multiple-testing burdens and risk overstating or misattributing causal effects driven by correlated pathways. Scalable methods that can accommodate many correlated exposures while providing valid inference are therefore urgently needed.

Several methods have been proposed to extend MVMR to high-dimensional settings, but each has important limitations. MR-BMA [21] uses Bayesian model averaging to prioritize likely causal factors but does not correct for weak instrument bias, which can compromise both estimation and selection. MVMR-cML-SuSiE [13] combines MVMR-cML with SuSiE to cluster exposures but assumes only one exposure per cluster has a direct effect. Both methods also require prespecifying the number of clusters or causal factors, which is typically unknown. Frequentist approaches include sparse principal component analysis [22], which constructs principal components from SNP-exposure associations but yields effects that are difficult to interpret biologically. Penalized regression approaches have also been developed. Grant and Burgess [17] estimate the effect of a primary exposure while applying an ℓ_1 penalty to select pleiotropic traits. Hao et al. [23] proposed a transfer learning framework that employs the Minimax Concave Penalty (MCP) for variable selection, which penalizes exposures individually but does not account for structured correlations or shared effects among exposures. However, both approaches fail to mitigate weak instrument bias. Critically, none of these methods provide valid post-selection inference, leaving statistical uncertainty poorly quantified after variable selection.

Here we introduce MVMR-PACS, a statistical framework for summary-data MVMR that addresses risk factor selection and post-selection inference in settings with many or highly correlated exposures. In such settings, disentangling individual causal effects is challenging because conditional instrument strength is limited. MVMR-PACS addresses this through three key innovations.

First, it mitigates weak instrument bias using a debiased loss function [11]. Second, it concentrates signal by adaptively grouping exposures that are genetically correlated or share causal effects through the pairwise absolute clustering and shrinkage (PACS) penalty [24]. Third, it estimates the causal effect of each group (Figure 1c), where the resulting estimand corresponds either to a common direct causal effect within the group or to a weighted average of member effects. For rigorous post-selection inference, we adapt the recently proposed data-thinning approach [25] to summary-data MVMR (Figure 1d). Compared with existing approaches, MVMR-PACS provides interpretable grouping of risk factors with theoretical guarantees for both estimation and inference after selection.

We establish that MVMR-PACS satisfies the oracle property for variable selection under reasonable conditions, ensuring consistent identification of true causal factors and signal-groups. Through simulations, we demonstrate its superior performance relative to existing methods in both estimation accuracy and variable selection. We then apply MVMR-PACS to 27 lipoprotein subfraction traits to identify biologically meaningful signal-groups influencing coronary artery disease risk and their direct causal effects.

2 Results

2.1 Overview of MVMR-PACS

To illustrate the MVMR-PACS workflow, we first provide a schematic overview before presenting simulation and applied analyses. We consider the widely used two-sample summary-data design, where SNP-exposure and SNP-outcome associations are obtained from non-overlapping cohorts. The framework begins by identifying SNPs that satisfy the three core instrument variable assumptions (Figure 1a). Candidate SNPs are selected based on association with at least one exposure at a specified significance threshold (for example, $p < 5 \times 10^{-8}$), followed by linkage disequilibrium clumping to retain independent variants (Figure 1b). The exposure and outcome datasets are then

harmonized to include only these instruments. Details of instrument variable selection and data preprocessing are provided in Methods (Section 4.3).

Using the harmonized dataset, MVMR-PACS identifies groups of risk factors that may jointly influence the outcome by combining exposures with high genetic correlation or indistinguishable causal effects. Figure 1c illustrates the approach using a hypothetical example with ten exposures. The correlation matrix of SNP-exposure associations reveals three clusters, though not all clusters contain causal exposures.

A key feature of MVMR-PACS is its ability to form signal-groups that capture both correlation structure and underlying causal effects in a data-driven manner. For instance, as illustrated in Figure 1c, risk factors 1–3 are highly correlated; the method shrinks their estimated effects toward a common value, even if their true effects differ slightly, recognizing that instrument strength is insufficient to distinguish them. Risk factors 4–6 are also highly correlated but non-causal; their estimated effects are correctly shrunk toward zero. Risk factors 7–10 exhibit weaker correlations and are treated as separate groups. We define a *signal-group* as a set of exposures assigned a nonzero estimated effect of equal magnitude. This grouping mitigates instability from multicollinearity, overcomes weak instrument bias by concentrating weak signals, and yields interpretable results.

The final step is inference on the identified signal-groups. To ensure valid post-selection inference, we adapt a data thinning strategy [25]. For each selected SNP, the vector of SNP-exposure associations is carefully perturbed to yield two independent components that preserve distributional properties of the original vector; SNP-outcome associations are treated analogously (Method Section 4.6). This procedure yields two independent datasets containing the same set of SNPs. One dataset is used for selection, where MVMR-PACS identifies signal-groups, and the other for inference, where direct effects and confidence intervals are estimated (Figure 1d). Unlike conventional sample-splitting approaches that partition SNPs into disjoint subsets [26, 27], data-thinning preserves all instruments in both datasets. This avoids instability when the number of instruments is limited while accommodating heterogeneous SNP-level association distributions.

The causal effect of a signal-group has a clear interpretation. When group members are highly

genetically correlated, the estimate reflects a weighted average of their individual effects. When weakly or moderately correlated members are grouped together, this indicates that the risk factors exert similar direct causal effects on the outcome, and the estimate reflects their common effect (Methods Section 4.5).

2.2 Simulation results

The simulation study evaluated the finite-sample performance of MVMR-PACS relative to existing MVMR estimators in terms of estimation accuracy and variable-selection performance. We also assessed whether the proposed data-thinning procedure yields valid post-selection inference. We generated summary-level data for ten risk factors under varying sample sizes to assess robustness to weak instruments. Results are summarized using 1,000 Monte Carlo replicates for each scenario.

The target estimand for each method was the direct causal effect of each exposure on the outcome. We compared MVMR-PACS and its variants—MVMR-PACS-0.8, which incorporates a correlation threshold of 0.8 to disable grouping between weakly correlated exposures, and MVMR-dLASSO, corresponding to the special case where the PACS penalty reduces to an ℓ_1 penalty—against several established estimators listed in Table 1.

Method performance was summarized using: (1) Estimation accuracy: median mean-squared error (MSE) across replicates, defined as the squared difference between estimated and true causal effects; (2) Variable selection performance: correct sparsity (proportion of exposures correctly identified as having zero or nonzero effects), sensitivity, and false-positive rate, accounting for direction of effect. To evaluate post-selection inference, we computed empirical coverage probability

Table 1: MVMR estimators compared in simulation and real-data analyses. Selection rules specify criteria for identifying exposures with nonzero direct causal effects on the outcome.

Method	Overview	Selection rule		
MVMR-IVW [15]	Inverse-variance weighted estimator assuming all instruments are valid and sufficiently strong.	Bonferroni-corrected $p < 0.05/K$ (K exposures).		
SRIVW [11]	$Weak-instrument-robust\ extension\ of\ MVMR-IVW.$	Bonferroni-corrected $p < 0.05/K$ (K exposures).		
IVW-LASSO (implemented in [21])	Adds an ℓ_1 penalty to MVMR-IVW for sparse estimation.	Selected if nonzero ¹ after penalization.		
MR-BMA [21]	Bayesian model averaging exploring likely exposure subsets; computes marginal inclusion probabilities (MIPs).	Selected if MIP > 0.2 , 0.5, or 0.8 (default: > 0.5).		
MVMR-cML- SuSiE [13]	Combines constrained maximum likelihood with SuSiE to identify causal clusters and estimate one effect per cluster.	Selected if exposure belongs to any causal cluster.		
MVMR-PACS	Adaptively group highly correlated exposures or those with indistinguishable causal effects and estimate each group's direct effect.	Selected if exposure belongs to any signal-group ¹ .		
MVMR-PACS-0.8	MVMR-PACS with a correlation threshold of 0.8; disabled grouping between exposures whose SNP-exposure associations have absolute correlation less than 0.8.	Selected if exposure belongs to any signal-group ¹ .		
MVMR-dLASSO	MVMR-PACS with grouping disabled, i.e., when the PACS penalty reduces to a usual ℓ_1 penalty.	Selected if nonzero ¹ after penalization.		

¹: Absolute values of estimated effects greater than 0.001.

of nominal 95% confidence intervals on the inference dataset, conditional on signal-groups identified in the selection dataset.

2.2.1 Estimation accuracy and risk factor selection

Figure 2 summarizes results across 1,000 replicates; numerical results are presented in Supplementary Table S1. At $N=1\times 10^5$, overall instrument strength was weak, with a mean instrument strength parameter [11] of -0.2 and conditional F-statistics [9] ranging from 1.1 to 13.1. The first three risk factors had mean conditional F-statistics of 1.1, indicating extremely weak conditional

instruments.

In this setting, MVMR-PACS achieved the lowest MSE and the most stable point estimates (Supplementary Figure S2). MR-BMA ranked second but frequently produced negative estimates for null effects (RF5, RF7, RF8, RF10), suggesting directional bias under weak instruments. MSE was not reported for MVMR-cML-SuSiE, as it evaluates all possible combinations of cluster representatives rather than producing a single set of exposure effects.

For variable selection, MVMR-PACS achieved the highest correct sparsity (88.3%), outperforming MR-BMA (75.3%), MVMR-cML-SuSiE (73.8%), and other methods. Its sensitivity reached 83.5%, compared with 86.2% for MR-BMA and 45.1% for MVMR-cML-SuSiE, while maintaining a low false-positive rate (8.5% versus 31.9% and 7.1%, respectively). False positives from MVMR-PACS mainly reflected moderate correlations between RF1-RF3 and RF4-RF6, where non-causal exposures (RF4-RF6) occasionally joined the same signal-group. When a correlation threshold (MVMR-PACS-0.8) was imposed, this grouping was prevented, yielding improved correct sparsity and reduced false-positive rates (Figure 2). These findings demonstrate how incorporating prior knowledge of risk factor group structure can enhance MVMR-PACS performance in practice.

IVW-LASSO achieved correct sparsity comparable to MVMR-PACS and MR-BMA but exhibited much larger MSE and lower sensitivity, especially at small sample sizes. MVMR-dLASSO showed even lower sensitivity, often selecting only one or two risk factors from RF1–RF3. SRIVW produced nearly unbiased estimates but with high variance, whereas MVMR-IVW displayed substantial bias and variability (Supplementary Figure S2). As expected, Bonferroni correction yielded conservative selection, with low sensitivity.

As sample size increased to 2×10^5 and 3×10^5 , performance improved for all estimators, with MVMR-PACS achieving the lowest MSE, highest correct sparsity, and highest sensitivity while maintaining a comparable false positive rate.

2.2.2 Post-selection Inference

We next examined whether the proposed data-thinning procedure yields valid confidence intervals conditional on the selection event. Using the same data-generation setup, we conducted 1,000 replications at each sample size $N=1\times 10^5$, 2×10^5 , and 3×10^5 . In each repetition, observed SNP-exposure and SNP-outcome associations were carefully perturbed to yield two independent datasets: a selection dataset, used by MVMR-PACS to identify signal groups, and an inference dataset, used for post-selection inference (Figure 1; Methods Section 4.6). Confidence intervals for the direct effects of the selected signal-groups were then constructed using the SRIVW estimator and evaluated against the true effects. In this setting, two signal-groups existed by design: one comprising RF1–RF3, which share the same true causal effect of 1, and another comprising RF9, with a true causal effect of 0.5.

Due to added noise and reduced instruments' strength in the selection dataset, MVMR-PACS exhibited slightly weaker performance than with full data (Supplementary Table S2). At sample size $N=1\times 10^5$, the most frequently observed grouping placed RF1–RF3 in a signal group, with remaining risk factors identified as non-causal. This grouping occurred in 775 of 1,000 runs. The number of runs in which MVMR-PACS correctly identified all causal risk factors increased with sample size: 132 at $N=1\times 10^5$, 342 at $N=2\times 10^5$, and 442 at $N=3\times 10^5$. The complete distribution of grouping frequencies is shown in Supplementary Table S3.

Coverage probabilities of SRIVW-based confidence intervals constructed on the inference set were close to the nominal 0.95 level when the correct model was selected (Supplementary Table S4).

2.3 Lipoprotein Subfraction Traits as Risk Factors for Coronary Artery Disease

2.3.1 Signal-groups identified by MVMR-PACS

We applied MVMR-PACS to traditional lipid profiles (HDL-C, LDL-C, TG, ApoA1, ApoB) and lipoprotein subfraction traits to identify signal-groups that may jointly influence coronary artery disease (CAD). We also applied the proposed data thinning technique to estimate group effects and construct confidence intervals.

Lipoprotein subfractions and particle sizes have gained increasing attention in cardiovascular risk assessment [28–31], yet observational studies have reported conflicting findings [12]. To address this, Zhao et al. [12] conducted an MR study of 82 traits spanning VLDL, LDL, IDL, and HDL subfractions and particle sizes. Each subfraction trait is named using three components separated by hyphens: size (XS, S, M, L, XL, XXL), lipoprotein density (VLDL, LDL, IDL, HDL), and measurement (C for total cholesterol, CE for cholesterol esters, FC for free cholesterol, L for total lipids, P for particle concentration, PL for phospholipids, TG for triglycerides). For example, M-HDL-P denotes the concentration of medium HDL particles. In addition, VLDL-D, LDL-D, and HDL-D represent the average diameters of the corresponding lipoprotein classes. After excluding traits with genetic correlations above 0.8 with traditional lipids, they retained 27 subfraction traits that may capture independent biological mechanisms, yet substantial correlations remained in the SNP-exposure associations. Consequently, each trait was analyzed separately while adjusting for traditional lipids, an approach that carries a high multiple testing burden and risks bias from uncontrolled pleiotropy since it is difficult to identify variants that affect a single subfraction without influencing others.

To overcome these limitations, we jointly analyzed the 27 subfraction traits and five traditional lipids using MVMR-PACS. Publicly available GWAS summary statistics were harmonized and inverse rank normalized to place all traits on the same scale (see Supplementary Section 2 for data sources). SNPs were first selected based on genome-wide significance ($p < 5 \times 10^{-8}$) for association

with at least one of the 32 lipid traits. Variants meeting this criterion were then clumped to ensure independence, using pairwise linkage disequilibrium ($r^2 < 0.001$) within a 10 Mb window and the European reference panel from the 1000 Genomes Project. Within each linkage disequilibrium block, the SNP showing the smallest p-value for association with any of the lipid traits was retained. This procedure yielded a total of 591 uncorrelated SNPs. The correlation matrix of SNP-exposure associations (Figure 3) showed a clear clustered structure. Conditional F-statistics for the 32 traits ranged from 0.16 to 1.31, and the instrument strength parameter was negative (-24.3), both indicating extremely weak instrument strength.

MVMR-PACS identified seven signal groups (Table 2), labeled by their members: TG; LDL-C; ApoB; HDL-D; medium/large HDL subfractions (M-HDL-CE, M-HDL-L, M-HDL-PL, M-HDL-PL, L-HDL-PL); LDL subfractions (S-LDL-C, S-LDL-L, S-LDL-P, M-LDL-CE, M-LDL-L, M-LDL-P, L-LDL-P); and a mixed VLDL/IDL/LDL group (XS-VLDL-L, XS-VLDL-PL, IDL-C, IDL-FC, IDL-L, L-LDL-FC, LDL-D). These groupings largely mirrored the correlation-based clusters yet also revealed separations driven by estimated causal effects. For example, despite their high correlation, ApoB and LDL-C formed distinct groups, whereas LDL-D clustered with VLDL/IDL lipid components despite weaker phenotypic correlation.

Based on the MVMR-PACS estimates, medium/large HDL subfractions, LDL subfractions, and LDL and HDL diameters showed protective effects on CAD risk, while LDL-C, ApoB, TG, VLDL/IDL subfractions, and L-LDL-FC indicated harmful effects. For groups with strong internal correlation (for example, the signal-group of LDL subfractions), estimates should be interpreted as weighted averages of member traits' effects; for signal-groups with weaker internal correlation (such as LDL-D with VLDL lipid components), the equal magnitude of effects suggests comparably sized causal effects (see Methods Section 4.5).

2.3.2 Other methods

For comparison, we applied six alternative MVMR estimators to the same dataset: MVMR-IVW, SRIVW, IVW-LASSO, MVMR-dLASSO, MR-BMA, and MVMR-cML-SuSiE (Table 2).

Estimates from MVMR-IVW and SRIVW were unstable, reflecting the extremely weak instrument strength. IVW-LASSO and MVMR-dLASSO agreed on LDL-C, TG and S-LDL-C, but disagreed on a few correlated traits.

For MR-BMA, the leading risk factors ranked by marginal inclusion probabilities (MIPs) were LDL-C (MIP = 1), TG (MIP = 0.996), ApoB (MIP = 0.989), L-LDL-P (MIP = 0.988), HDL-D (MIP = 0.975), and L-HDL-PL (MIP = 0.967) (Supplementary Table S6). Notably, MR-BMA produced a model-averaged causal effect estimate for ApoB of -0.497, which likely reflects weak instrument bias and contradicts the established consensus that elevated ApoB increases CAD risk [32].

MVMR-cML-SuSiE identified three clusters: cluster 1 (LDL-C), cluster 2 (ApoA1 and HDL-C), and cluster 3 (L-LDL-FC, IDL-L, IDL-FC, IDL-C). A representative risk factor from each cluster was then selected, yielding eight possible models. MVMR-cML was applied to each model to estimate causal effects (numerical results are presented in Supplementary Table S7). LDL-C and the cluster of ApoA1 and HDL-C consistently showed harmful effects, whereas risk factors in clusters 3 suggested protective effects. However, despite accounting for collinearity through cluster selection, the point estimates are likely biased by residual pleiotropy, as only one exposure from each cluster is retained for analysis. For example, LDL-C exhibited an estimated effect size of approximately 2.2, corresponding to an 9-fold increase in CAD risk per standard deviation increase in LDL-C levels, far exceeding estimates from other approaches.

2.3.3 Inference with data thinning

We next applied the proposed data-thinning procedure, which splits the data into two independent copies, one for variable selection and the other for estimation and inference. As with many resampling approaches, random variation can affect results, particularly in settings with weak and noisy signals. To stabilize inference, we repeated the data thinning procedure 100 times.

Figure 4 shows a combined heatmap and dendrogram summarizing MVMR-PACS estimates across 100 data thinning replicates. The heatmap displays effects for the 32 traits that were

nonzero and statistically significant at p < 0.05. Across runs, LDL-C, TG, XS-VLDL-PL, and XS-VLDL-L consistently showed harmful effects, while small and medium LDL subfractions and medium HDL subfractions showed protective effects, with concordant significance in more than half of the replicates. These directions also matched the primary full-data results (Table 2). Other traits were either not significant in most runs or showed inconsistent directions, indicating limited and unstable evidence of causal effects.

The dendrogram visualizes clustering of the 32 traits using a custom distance metric defined by the frequency of co-assignment to the same signal-group across runs. Traits that repeatedly grouped together clustered tightly. Several signal-groups from the full-data analysis, including medium HDL subfractions, small and medium LDL subfractions, VLDL lipid components were frequently recovered. In contrast, LDL-C and TG were often isolated into distinct groups, consistent with the full-data analysis in Table 2.

3 Discussion

We introduced MVMR-PACS, a general framework for risk factor selection and post-selection inference in summary-data MVMR. The method expands the current toolbox to settings with many, often highly correlated, risk factors. By minimizing a debiased objective function that accounts for the clustered structure of SNP-exposure associations, MVMR-PACS provides principled estimation and transparent grouping. It adaptively identifies clusters of risk factors with high correlation or indistinguishable effects, and interprets the direct effect of a signal-group as a weighted average of its members' causal effects. When risk factors are not highly correlated, or when there is sufficient instrument strength to distinguish their individual effects, MVMR-PACS treats them as distinct signal groups. This adaptive, data-driven behavior makes MVMR-PACS broadly applicable. We formally demonstrate that MVMR-PACS exhibits the oracle property of variable selection: it can consistently identify causal risk factors in the presence of many weak instruments (Methods, Section 4.8).

To address the challenge of inference following risk factor selection, we extended the data thinning approach to summary-data MVMR. This approach generates independent analytic datasets of summary statistics that retain the same number of SNPs as the original dataset while preserving key information necessary for both causal effect estimation and signal group identification. By using one dataset for signal group identification and an independent dataset for inference, our method yields valid post-selection inference when the true model is correctly identified. Moreover, this approach is broadly applicable to other tasks in MVMR studies, such as cross-validation, where traditional sample-splitting based on available instruments may be infeasible or inappropriate. Therefore, it serves as a valuable tool that complements existing methods in the MVMR literature.

Our method has several limitations. First, signal groups identified by MVMR-PACS may comprise heterogeneous components without feasible intervention targets to modify the entire group. We therefore advise against interpreting the estimated direct effect of a signal group in the traditional way—as the effect of a unit change in the exposure on the outcome. Instead, the effect should be viewed as a weighted average of the direct causal effects of the risk factors within the group. A nonzero group effect indicates the presence of at least one true causal risk factor, but disentangling individual contributions will likely require new data and methods beyond MR.

Second, although Theorem 1 establishes that MVMR-PACS enjoys the oracle property for risk factor selection in the presence of many weak instruments, this guarantee relies on specific conditions. A sufficient condition is that, as sample size grows, the ratio $\mu_{n,\min}/\sqrt{p} \to \infty$, where p is the number of instruments and $\mu_{n,\min}/\sqrt{p}$ is the instrument strength parameter defined in Wu et al. [11]. This parameter reflects the weakest instrument strength across all linear combinations of exposures and serves as a diagnostic measure for estimators such as MVMR-IVW or SRIVW that aim to estimate each exposure's direct effect. In practice, one can compute its empirical value, $\hat{\mu}_{n,\min}/\sqrt{p}$; values smaller than the rule-of-thumb threshold of 7, or negative values, indicate potential weak-instrument bias, as observed in our data application. However, this does not necessarily imply failure of MVMR-PACS. Unlike estimators that attempt to recover all individual

exposure effects, MVMR-PACS adaptively aggregates highly correlated exposures or those with indistinguishable effects into signal groups, thereby mitigating instability from extremely weak instruments while still producing accurate estimates for groups with adequate conditional instrument strength. Additionally, our simulation study shows that MVMR-PACS maintains low MSE and good variable selection performance even when $\hat{\mu}_{n,\text{min}}/\sqrt{p} < 0$, indicating that the instrument strength condition is sufficient but not necessary for satisfactory finite-sample performance. These observations suggest that the formal instrument-strength condition may be stronger than necessary for MVMR-PACS, since its practical goal in settings with highly correlated exposures is not to disentangle every individual effect but to identify and estimate interpretable signal groups. Relaxing this requirement remains an important direction for future work.

Third, as with any variable-selection method, MVMR-PACS may fail to correctly identify all signal-groups. This limitation reflects a fundamental challenge rather than a specific shortcoming of the method: when the available instruments contain insufficient independent information, no data-driven approach can fully separate highly correlated causal signals. Nevertheless, MVMR-PACS provides a transparent framework that allows users to incorporate prior knowledge to improve stability. The PACS penalty can be customized by setting selected pairwise weights to zero to prevent grouping between specific traits, or by assigning large positive weights to enforce grouping. As shown in Section 2.3, adjusting the correlation threshold is another way to influence the resulting group structure. This flexibility enables domain expertise to guide the grouping process, ensuring that the resulting signal-groups reflect both empirical and biological evidence rather than relying solely on data-driven process.

In practice, one can diagnose whether MVMR-PACS has likely identified reliable signal-groups through reasonable perturbations of data, such as repeated data-thinning runs or bootstrap resamples. Stable group membership indicates robust clustering. Conversely, highly variable group composition across runs suggests uncertainty due to weak instruments or collinearity.

Fourth, data thinning, used for both tuning parameter selection in MVMR-PACS and postselection inference, introduces randomness when generating independent copies of the dataset, which may affect performance and signal-group identification. To ensure stability and reproducibility, we recommend repeating the procedure multiple times. For example, in tuning parameter selection, a five-fold data thinning procedure can be repeated several times, and the tuning parameter that minimizes the average loss across runs selected. This process can be parallelized to reduce computation time.

Summarizing post-selection inference across repeated runs is more nuanced, as signal-groups may vary slightly between iterations and the literature provides little guidance on how to integrate such results. We explored two strategies. The first is to focus on the most frequently observed grouping and compute the median of point estimates and standard errors for each signal-group across runs, from which confidence intervals and p-values are derived. A caveat is that datasets are independent within runs but not across runs. In addition, when instrument strength is very weak, signal-group identification may be inconsistent across repeated runs, and the most frequent grouping may not represent the most plausible structure. The second strategy, which we recommend in practice, is to descriptively summarize variation in groupings and inference results, for example using a heatmap as in Figure 4. A similar approach was adopted by Dharamshi et al. [33] to assess the stability of changepoint detection with data thinning.

Fifth, the confidence intervals constructed using our data thinning procedure are valid only if MVMR-PACS correctly identifies all signal-groups. Our theoretical results show that MVMR-PACS can consistently recover the true signal-groups under appropriate conditions (Methods, Section 4.8), a finding further supported by our simulations. These results suggest that the confidence intervals are asymptotically valid. In finite samples, however, failure to identify the correct model can lead to misspecification in the inference stage, resulting in invalid confidence intervals.

In summary, MVMR-PACS extends the methodological toolkit for high-dimensional MR by integrating principled risk factor selection with valid post-selection inference. By explicitly accounting for correlation among exposures and addressing the challenges posed by weak instruments, the framework provides a robust approach for disentangling complex causal relationships, particularly in genomic and molecular data.

4 Methods

4.1 Model and identification

We consider the problem of estimating the causal effects of K potentially correlated exposures $\mathbf{X} = (X_1, ..., X_K)^T$ on an outcome Y, in the presence of unmeasured confounders \mathbf{U} . Let $\mathbf{Z} = (Z_1, ..., Z_p)^T$ denote p independent SNPs, obtained through linkage disequilibrium (LD) pruning or clumping [34], which satisfy the three instrument assumptions. The causal model is given by

$$\Gamma_j = \gamma_{j1}\beta_1^* + \gamma_{j2}\beta_2^* + \dots + \gamma_{jK}\beta_K^*, \quad j = 1,\dots, p$$
(1)

where Γ_j is the marginal SNP-outcome association, γ_{jk} is the marginal SNP-exposure association for exposure k, and β_k^* is the direct effect of exposure X_k on Y. This formulation arises from the structural equations

$$X_k = \sum_{j=1}^p Z_j \gamma_{jk} + f_k(\mathbf{U}, E_{Xk}), \quad k = 1, \dots, K,$$
 (2)

$$Var(X_k) = 1, \quad k = 1, \dots, K,$$
(3)

$$Y = \mathbf{X}^T \boldsymbol{\beta}^* + g(\mathbf{U}, E_Y), \tag{4}$$

where $\boldsymbol{\beta}^* = (\beta_1^*, \beta_2^*, ..., \beta_K^*)^T$, E_Y is a random noise term, (E_Y, \boldsymbol{U}) is independent of \boldsymbol{Z} by the second instrument assumption, and $f_1, ..., f_K, g$ are unspecified functions. We scale the exposures to unit variance so that the elements of $\boldsymbol{\beta}^*$ are comparable. The causal model in (1) remains approximately correct even when model (4) is nonlinear, for example when Y is binary or when \boldsymbol{X} has nonlinear effects on Y [18, 35]. In such cases, $\boldsymbol{\beta}^*$ represents average local effects of the exposures. From (1), $\boldsymbol{\beta}^*$ is uniquely identified provided that the design matrix

$$\Pi = \begin{bmatrix} \gamma_{11} & \dots & \gamma_{1K} \\ \vdots & \ddots & \vdots \end{bmatrix} \\
\gamma_{p1} & \dots & \gamma_{pK}$$
(5)

has full column rank. In the following, we use γ_j , j = 1, ..., p, to denote its rows.

We focus on settings with many potentially correlated risk factors, where K is large but fixed and the matrix Π may suffer from multicollinearity. In such cases, standard MVMR estimators

can be unstable and biased, particularly when estimation error in $\hat{\Pi}$ is large.

4.2 Two-sample summary-data MVMR

Our framework is based on the two-sample summary-data MVMR setting, in which SNP-exposure and SNP-outcome associations are obtained from non-overlapping GWASs, while allowing for sample overlap across the exposure datasets. For each SNP j = 1, ..., p, we observe the vector of estimated SNP-exposure associations $\hat{\gamma}_j = (\hat{\gamma}_{j1}, ..., \hat{\gamma}_{jK})^T$ from marginal regressions of each standardized exposure on SNP j, along with their standard errors $(\sigma_{Xj1}, ..., \sigma_{XjK})^T$. We also observe the SNP-outcome association estimate $\hat{\Gamma}_j$ from the marginal regression of the outcome Y on SNP j, together with its standard error σ_{Yj} .

To account for potential sample overlap between exposure GWASs, we incorporate a shared positive-definite correlation matrix Σ , which captures correlations among elements of $\hat{\gamma}_j$. The variance-covariance matrix of $\hat{\gamma}_j$ is

$$\Sigma_{Xj} = \operatorname{diag}(\sigma_{Xj1}, ..., \sigma_{XjK}) \Sigma \operatorname{diag}(\sigma_{Xj1}, ..., \sigma_{XjK}).$$

Although Σ is not directly available from GWAS summary statistics, it can be estimated using bivariate LD score regression [36] or from empirical correlations between GWAS Z-scores across null SNPs [18].

Given the large sample sizes in modern genome-wide association studies, we assume for each SNP j, $\hat{\gamma}_j \sim N(\gamma_j, \Sigma_{X_j})$ and $\hat{\Gamma}_j \sim N(\Gamma_j, \sigma_{Y_j}^2)$ (see Assumption 1 in Supplement).

4.3 Instrument Selection and Data Preprocessing

We followed the approach of [18] to select p SNPs associated with at least one risk factor at a genome-wide significance threshold of 5×10^{-8} . After initial screening, LD clumping was applied to obtain a set of approximately independent SNPs, a procedure demonstrated in our data application. When risk factors are measured on different scales, we recommend rescaling SNP-exposure associations and their standard errors by the reported standard deviation of each risk factor, en-

suring that all estimated causal effects are comparable.

Throughout, we assume that the number of SNPs exceeds the number of risk factors and that these SNPs satisfy the instrumental variable assumptions. In practice, additional filtering methods [13, 37] can be incorporated during SNP selection to help exclude potentially invalid instruments and reduce the risk of violating the exclusion restriction.

4.4 MVMR-PACS

We propose MVMR-PACS, a novel estimator for MVMR designed for settings with many highly correlated risk factors. Unlike existing methods, MVMR-PACS explicitly accounts for the fact that $\hat{\Pi}$ is a random matrix with entries measured with error.

Most existing MVMR estimators ignore this source of uncertainty. For example, the widely used inverse-variance weighted (IVW) estimator [15] minimizes

$$\mathcal{L}_{\text{IVW}}(\boldsymbol{\beta}) = \frac{1}{2} (\hat{\boldsymbol{\Gamma}} - \hat{\boldsymbol{\Pi}} \boldsymbol{\beta})^T W (\hat{\boldsymbol{\Gamma}} - \hat{\boldsymbol{\Pi}} \boldsymbol{\beta})$$
$$= \frac{1}{2} \boldsymbol{\beta} \hat{\boldsymbol{\Pi}}^T W \hat{\boldsymbol{\Pi}} \boldsymbol{\beta} - \hat{\boldsymbol{\Gamma}}^T W \hat{\boldsymbol{\Pi}} \boldsymbol{\beta} + c, \tag{6}$$

where $\hat{\mathbf{\Gamma}} = (\hat{\Gamma}_1, ..., \hat{\Gamma}_p)$, $W = \text{diag}(1/\sigma_{Y1}^2, ..., 1/\sigma_{Yp}^2)$ and c is a constant independent of $\boldsymbol{\beta}$. The IVW estimator is known to suffer bias when instruments are weak [11]. This bias arises because the loss function it minimizes differs from the oracle form,

$$\mathcal{L}_{\text{IVW}}^{\text{oracle}}(\boldsymbol{\beta}) = \frac{1}{2} \boldsymbol{\beta} \Pi^T W \Pi \boldsymbol{\beta} - \hat{\boldsymbol{\Gamma}}^T W \Pi \boldsymbol{\beta} + c, \tag{7}$$

with the discrepancy between Π and its estimate $\hat{\Pi}$ driving the bias when estimation error in $\hat{\Pi}$ is non-negligible.

To address this, we debias the IVW loss by noting that

$$E(\hat{\Pi}^T W \hat{\Pi}) = \Pi^T W \Pi + V, \quad E(\hat{\Gamma}^T W \hat{\Pi}) = \Gamma^T W \Pi,$$

where $V = \sum_{j=1}^{p} \sum_{X_j} \sigma_{Y_j}^{-2}$. Minimizing the debiased loss function,

$$\mathcal{L}_{\text{debiased}}(\boldsymbol{\beta}) = \frac{1}{2} \boldsymbol{\beta}^T (\hat{\Pi}^T W \hat{\Pi} - V) \boldsymbol{\beta} - \hat{\boldsymbol{\Gamma}}^T W \hat{\Pi} \boldsymbol{\beta}, \tag{8}$$

is, on average, equivalent to minimizing the oracle loss in (7). When $(\hat{\Pi}^T W \hat{\Pi} - V)$ is positive

definite, this yields the debiased IVW estimator [11].

A challenge arises when $(\hat{\Pi}^T W \hat{\Pi} - V)$ is not positive definite, in which case the loss is non-convex and unbounded below. To restore convexity, we adopt the projection technique of [38] and define the projected debiased loss function:

$$\mathcal{L}_{\text{debiased}}^{+}(\boldsymbol{\beta}) = \frac{1}{2} \boldsymbol{\beta}^{T} (\hat{\Pi}^{T} W \hat{\Pi} - V)_{+} \boldsymbol{\beta} - \hat{\boldsymbol{\Gamma}}^{T} W \hat{\Pi} \boldsymbol{\beta}, \tag{9}$$

where $(M)_+$ denotes the nearest positive semi-definite matrix to M, computed as

$$(M)_{+} = \underset{M'>0}{\arg\min} ||M - M'||_{\max}, \tag{10}$$

where M' is any positive definite matrix and $||M||_{\max} = \max_{i,j} |M_{ij}|$ denotes the elementwise maximum norm. This projection ensures convexity and stability by discarding information along directions in which causal effects are effectively unidentified (e.g., contrasts between almost collinear exposures), while preserving information in directions with sufficient instrument strength.

Building on this projected debiased loss, we define the MVMR-PACS estimator $\hat{\beta}_{PACS}$ as the minimizer of

$$\mathcal{L}_{PACS}(\boldsymbol{\beta}, \lambda) = \frac{1}{2} \boldsymbol{\beta}^{T} (\hat{\Pi}^{T} W \hat{\Pi} - V)_{+} \boldsymbol{\beta} - \hat{\Gamma}^{T} W \hat{\Pi} \boldsymbol{\beta}$$

$$+ \lambda \left\{ \sum_{k=1}^{K} w_{k} |\beta_{k}| + \sum_{k < m} w_{km(-)} |\beta_{k} - \beta_{m}| + \sum_{k < m} w_{km(+)} |\beta_{k} + \beta_{m}| \right\}, \tag{11}$$

where λ is a tuning parameter and w_k , $w_{km(-)}$, and $w_{km(+)}$ are non-negative weights. Alternative forms of penalization are reviewed in Supplementary Section 3. The PACS penalty is particularly attractive because it adapts to the correlation structure of the exposures and does not require prior specification of grouping.

We adopt adaptive weighting schemes following [24]. The weights depend on an initial consistent estimator and the observed correlations \hat{r}_{km} between SNP-exposure associations for exposures k and m. The weights are defined as

$$w_k = |\tilde{\beta}_k|^{-\tau}, \quad w_{km(-)} = (1 - \hat{r}_{km})^{-\tau} |\tilde{\beta}_k - \tilde{\beta}_m|^{-\tau}, \quad w_{km(+)} = (1 + \hat{r}_{km})^{-\tau} |\tilde{\beta}_k + \tilde{\beta}_m|^{-\tau}$$

for k, m = 1, ..., K, where $\tilde{\beta}_{\text{init}} = (\tilde{\beta}_1, ..., \tilde{\beta}_K)^T$ is a consistent and asymptotically normal initial

estimator of β under the conditions of Theorem 1, and τ is another tuning parameter. This construction ensures weaker penalization for effects or pairwise sums/contrasts that are large in magnitude, a critical feature for achieving the oracle property [24, 39]. Tuning parameters are selected using multi-fold data thinning (see Sections 4.6).

By incorporating correlations between SNP-exposure associations, MVMR-PACS shrinks coefficients toward each other more heavily when \hat{r}_{km} is close to one, or toward opposite values when \hat{r}_{km} is close to minus one. This improves stability in the presence of highly correlated exposures that cannot be disentangled due to weak conditional instruments. When associations are not highly correlated, the method estimates each risk factor's effect individually.

We use the minimizer of $\mathcal{L}_{\text{debiased}}^+(\beta)$ with a ridge penalty as the initial estimator (its consistency and asymptotic normality are established in Supplementary Section 8) and then minimize $\mathcal{L}_{\text{PACS}}(\beta, \lambda)$ using the local quadratic approximation algorithm of Sharma et al. [24], which provides efficient closed-form updates (see Supplementary Section 7 for details). When $w_{km(-)} = w_{km(+)} = 0$, the PACS penalty reduces to the adaptive LASSO penalty [39], yielding the MVMR-dLASSO estimator. As illustrated by MVMR-PACS-0.8 in our simulation study, we also consider a family of variants, denoted MVMR-PACS-x, which incorporate a correlation threshold of value x into the weighting scheme to control the degree of grouping among correlated exposures (see Supplementary Section 5 for details).

4.5 Signal-groups and estimand from MVMR-PACS

MVMR-PACS produces clusters of exposures, which we refer to as *signal-groups*. A signal-group is defined as a set of risk factors that share nonzero effect estimates of equal magnitude (up to a specified decimal precision). Each signal-group can be viewed as a linear combination—typically a sum or difference—of the risk factors it contains, with the direction determined by the signs of their estimated effects. The key question is how to interpret the shared effect for each signal-group.

To illustrate, consider $K_1 + K_2$ exposures. Suppose MVMR-PACS identifies two signal-groups: G_1 , comprising the first K_1 exposures, and G_2 , comprising the remaining K_2 . A working model

then estimates the direct causal effects of G_1 and G_2 . As shown in Supplementary Section 4, these effects are linear combinations of the true causal effects of all exposures, including those outside the respective groups. The grouping becomes interpretable when the exposures within a signal-group are strongly correlated in their SNP-exposure associations or genuinely share the same causal effect, in which case the estimated group effect approximates a weighted average of the individual effects with positive weights.

When multicollinearity is severe, the true model may be unidentifiable, making the working model not only a pragmatic approximation but also a necessary alternative for stable estimation. Indeed, existing high-dimensional MVMR methods also rely on working models for effect estimation and variable selection. For example, MR-BMA averages over many combinations of risk factors, and MVMR-cML-SuSiE selects representative exposures from causal clusters. Each combination implicitly defines a working model. However, these approaches provide limited discussion of how to interpret the resulting estimands or of the conditions under which such working models approximate the true model.

4.6 Data thinning for summary-data MVMR

We introduce a data-thinning approach [25] to generate independent replicates of GWAS summary statistics, which can then be used for tasks such as cross-validation and post-selection inference.

In the MVMR literature, cross-validation is often implemented by sample splitting, where SNPs are randomly partitioned into folds [26, 27]. This approach is often infeasible when the number of instruments is small and SNP-level association distributions are heterogeneous. For post-selection inference, existing approaches generally use the same dataset for both model selection and inference, which can result in underestimated standard errors and inflated type I error due to "double dipping." Although this limitation has been noted in prior work [13, 26], it remains unresolved.

Data thinning provides a way forward [25]. The idea is to decompose an observed SNP–exposure or SNP–outcome association into two or more independent parts that sum to the original estimate

while retaining the same distributional structure, up to a known scaling factor. For example, in two-fold thinning, for each SNP j one can create two independent SNP-exposure association estimates by

$$\hat{\pmb{\gamma}}_j^{(1)} = rac{\hat{\pmb{\gamma}}_j}{2} + \epsilon_j, \qquad \hat{\pmb{\gamma}}_j^{(2)} = \hat{\pmb{\gamma}}_j - \hat{\pmb{\gamma}}_j^{(1)},$$

where ϵ_j is drawn independently from $N(0, \frac{\Sigma_{X_j}}{4})$, so that marginally,

$$\hat{\gamma}_j^{(1)} \sim N(\frac{\gamma_j}{2}, \frac{\Sigma_{Xj}}{2}), \qquad \hat{\gamma}_j^{(2)} \sim N(\frac{\gamma_j}{2}, \frac{\Sigma_{Xj}}{2}),$$

with $\hat{\gamma}_j^{(1)}$ and $\hat{\gamma}_j^{(2)}$ independent. SNP-outcome associations can be decomposed analogously. The resulting two independent datasets, $\left\{\hat{\gamma}_j^{(1)}, \Sigma_{Xj}/2, \hat{\Gamma}_j^{(1)}, \sigma_{Yj}^2/2, j=1,...,p\right\}$ and $\left\{\hat{\gamma}_j^{(2)}, \Sigma_{Xj}/2, \hat{\Gamma}_j^{(2)}, \sigma_{Yj}^2/2, j=1,...,p\right\}$, each contain all p SNPs and preserve the causal relationship in equation (1), while providing independent replicates for downstream analysis. The main consequence of generating independent replicates is a reduction in instrument strength. As shown in Supplementary Section 6, the instrument strength parameter [11] is halved under standard two-fold thinning, making it necessary to use weak-instrument robust methods for inference.

Although the above procedure partitions data into two parts, it can be extended to create M independent datasets with potentially uneven information allocation, a strategy we refer to as multi-fold data thinning. A general procedure for multi-fold thinning in MVMR is provided in Supplementary Section 6.

4.7 Cross-validation

We use five-fold data thinning and select tuning parameters by minimizing the projected debiased loss function

$$\sum_{i=1}^{5} \frac{1}{2} \hat{\boldsymbol{\beta}}_{-i}(\boldsymbol{\delta})^{T} (\hat{\Pi}_{i}^{T} W_{i} \hat{\Pi}_{i} - V_{i})_{+} \hat{\boldsymbol{\beta}}_{-i}(\boldsymbol{\delta}) - \hat{\boldsymbol{\Gamma}}_{i}^{T} W_{i} \hat{\Pi}_{i} \hat{\boldsymbol{\beta}}_{-i}(\boldsymbol{\delta}), \tag{12}$$

where $\boldsymbol{\delta} = (\lambda, \tau)$ denotes the vector of tuning parameters, $\hat{\Pi}_i$, W_i , V_i , $\hat{\Gamma}_i$ are based on the *i*th replicate of the summary statistics, and $\hat{\boldsymbol{\beta}}_{-i}(\boldsymbol{\delta})$ is obtained based on the summary statistics summed over the remaining replicates (see Supplementary Section 6).

In high-dimensional settings, parsimony is often desirable. To encourage simpler models, we apply the one-standard-error (1SE) rule. After computing the cross-validated loss for a grid of candidate tuning parameter values, we identify the parameter choice that minimizes the average loss and calculate the corresponding standard error. Among all candidates whose average loss lies within one standard error of the minimum, we first select the largest λ , then the largest τ among candidates sharing that λ value. This strategy promotes sparsity and grouping of correlated risk factors while maintaining near-optimal predictive accuracy, thereby mitigating overfitting and reducing false discoveries. Choices of λ and τ are further discussed in the next section, where we present the theoretical results.

4.8 Theoretical analysis

4.8.1 MVMR-PACS

We establish that MVMR-PACS enjoys the oracle properties of variable selection and signal-group identification. Let $\beta^* = (\beta_1^*, \beta_2^*, \dots, \beta_{K_1}^*, \beta_{K_1+1}^*, \dots, \beta_{K_1+K_0}^*)^T$ denote the vector of true causal effects for $K = K_1 + K_0$ risk factors, where the first K_1 are causal $(\beta_k^* \neq 0 \text{ for } k = 1, \dots, K_1)$ and the remaining K_0 are non-causal. Suppose the causal risk factors can be partitioned into signal-groups $\mathcal{G} = \{G_1, \dots, G_L\}$ such that within each group G_l all effects share the same magnitude, $|\beta_k^*| = \alpha_l$ for $k \in G_l$, with $\alpha_l > 0$. Since signs may differ within a group, we write $\beta_k^* = s_k \alpha_l$ for $k \in G_l$, where $s_k \in \{-1, +1\}$ denotes the sign.

To uniquely represent grouped effects, we define a canonical representative for each group. For l = 1, ..., L, let $k_l = \min\{k : k \in G_l\}$ denote the smallest index in group G_l , and set the group sign as $\bar{s}_l = s_{k_l} \in \{-1, +1\}$. We then construct an $L \times K$ matrix C_g with entries

$$C_{g,lk} = \begin{cases} \frac{\bar{s}_l s_k}{|G_l|}, & k \in G_l \\ 0, & \text{otherwise} \end{cases},$$

where $|G_l|$ is the size of group G_l . The grouped causal effects are defined as $\bar{\beta}^* = (\bar{\beta}_1^*, \dots, \bar{\beta}_L^*)^T =$

 $C_q \boldsymbol{\beta}^* \in \mathbb{R}^L$, with

$$\bar{\beta}_l^* = \frac{\bar{s}_l}{|G_l|} \sum_{k \in G_l} s_k \beta_k^*.$$

As an illustration, consider five risk factors with $\beta_1^* = \beta_2^*$, $\beta_3^* = -\beta_4^*$, and $\beta_5^* = 0$, where $|\beta_1| \neq |\beta_3|$. This yields three groups (two causal and one non-causal) and the grouping matrix

$$C_g = \begin{bmatrix} 0.5 & 0.5 & 0 & 0 & 0 \\ 0 & 0 & 0.5 & -0.5 & 0 \end{bmatrix},$$

which maps β^* to the group-level effects $\bar{\beta}^*$ and drops the exposures with no effects.

To study the consistency of variable selection and group identification, we follow [24] and define the over-parameterized vector $\boldsymbol{\theta}^* = M\boldsymbol{\beta}^*$, where M is a $K^2 \times K$ matrix given by $M = [I_K \ D_{(-)}^T \ D_{(+)}^T]^T$. The matrix $D_{(-)}$ has dimension $\frac{K(K-1)}{2} \times K$ with entries ± 1 , such that $D_{(-)}\boldsymbol{\beta}$ yields all pairwise differences of $\boldsymbol{\beta}$ (for example, $\beta_2 - \beta_1, \beta_3 - \beta_1, \ldots, \beta_K - \beta_{K-1}$). Similarly, $D_{(+)}$ is a $\frac{K(K-1)}{2} \times K$ matrix with entries equal to +1, such that $D_{(+)}\boldsymbol{\beta}$ gives all pairwise sums of $\boldsymbol{\beta}$.

Let $\mathcal{B} = \{k : \theta_k^* \neq 0, k = 1, ..., K^2\}$ denote the set of nonzero indices of $\boldsymbol{\theta}^*$. Its complement, \mathcal{B}^c , specifies which risk factors have no causal effects and which share effects of identical magnitude and direction, thereby defining the oracle sparsity pattern and grouping structure. Let $\mathcal{B}_n = \{k : \hat{\theta}_k^* \neq 0, k = 1, ..., K^2\}$ denote the corresponding set estimated by MVMR-PACS, where $\hat{\boldsymbol{\theta}}^* = M\hat{\boldsymbol{\beta}}_{PACS}$ and $\hat{\boldsymbol{\beta}}_{PACS}$ is defined in equation (11).

Let $\bar{\gamma}_j = G\gamma_j$ denote the true association of SNP j with the L causal groups, where G is an $L \times K$ matrix analogous to C_g but without the $|G_l|$ scaling. Specifically,

$$G_{lk} = \begin{cases} \bar{s}_l s_k, & k \in G_l \\ 0, & \text{otherwise} \end{cases},$$

so that G collapses elements of γ_j : it sums those with nonzero effects of the same magnitude and direction, subtracts those with opposite effects, and omits those with zero effects.

Theorem 1. (Oracle properties of MVMR-PACS) Under the standard MVMR Assumptions 1-2 (see Supplementary Section 8), if $\mu_{n,\min}/\sqrt{p} \to \infty$ and $\max_j \gamma_{jk}^2 \sigma_{Xjk}^{-2}/(\mu_{n,\min}+p) \to 0$ for all k as

 $n \to \infty$, and if the tuning parameters satisfy $\lambda_n/r_n \to 0$, $\lambda_n r_n^{\tau-1} \to \infty$ with $r_n = \mu_{n,\min}/\sqrt{\mu_{n,\min} + p}$ and $\lambda_n r_n^{\tau+1}/\mu_{n,\max} \to \infty$, then the MVMR-PACS estimator has the following properties:

- 1. Consistency in risk factor selection: $\lim_n \mathbb{P}(\mathcal{B}_n = \mathcal{B}) = 1$.
- 2. Asymptotic normality: $\mathbb{V}_g^{-\frac{1}{2}}(\Pi_q^T W \Pi_g)(C_g \hat{\boldsymbol{\beta}}_{PACS} C_g \boldsymbol{\beta}^*) \xrightarrow{D} N(\mathbf{0}, I_L).$

Here,
$$\mathcal{B} = \{k : \theta_k \neq 0, k = 1, ..., K^2\}$$
, $\mathcal{B}_n = \{k : \hat{\theta}_k^* \neq 0\}$, $\Pi_g = \Pi G^T$, $V_{j,g} = G \Sigma_{Xj} \sigma_{Yj}^{-2} G^T$, $\mathbb{V}_g = \sum_{j=1}^p \{(1 + \bar{\boldsymbol{\beta}}^{*T} V_{j,g} \bar{\boldsymbol{\beta}}^*) (G \boldsymbol{\gamma}_j \boldsymbol{\gamma}_j^T \sigma_{Yj}^{-2} G^T + V_{j,g}) + V_{j,g} \bar{\boldsymbol{\beta}}^* \bar{\boldsymbol{\beta}}^{*T} V_{j,g} \}$, with I_L denoting the $L \times L$ identity matrix.

The proof is provided in the Supplement. Assumptions 1 and 2 are standard and were also used in [11]. The scalar $\mu_{n,\min}$ is an instrument strength parameter that characterizes the rate at which instrument strength increases along the weakest direction among all linear combinations of exposures as $p \to \infty$, which determines the asymptotic behavior of MVMR estimators. The condition $\max_j(\gamma_{jk}^2\sigma_{Xjk}^{-2})/(\mu_{n,\min}+p) \to 0$ for all k ensures that no single SNP dominates the instrument strength and is required to verify Lindeberg's condition for the central limit theorem. The requirement $\mu_{n,\min}/\sqrt{p} \to \infty$ sets a minimum instrument strength condition needed for consistency and asymptotic normality of the initial estimator. By contrast, Wu et al. [11] showed that MVMR-IVW requires the stronger condition $\mu_{n,\min}/p^2 \to \infty$ to achieve consistency, which is generally impractical. Thus, $\mu_{n,\min}/\sqrt{p} \to \infty$ represents a substantially weaker and more realistic condition on instrument strength.

The additional requirements $\lambda_n/r_n \to 0$, $\lambda_n r_n^{\tau-1} \to \infty$, and $\lambda_n r_n^{\tau+1}/\mu_{n,\max} \to \infty$ are conditions on the tuning parameters. One regime where these conditions are satisfied is when $\mu_{n,\min} = \Theta(p)$, a typical rate under many weak instruments. We write $a = \Theta(b)$ if there exists a constant c > 0 such that $c^{-1}b \le |a| \le cb$. In this setting, $r_n = \Theta(\sqrt{p})$ and $\lambda_n = o(\sqrt{p})$. The maximum strength parameter $\mu_{n,\max}$ typically grows no faster than $\Theta(n)$, and in most MVMR studies it is reasonable to assume $n = O(p^2)$. Under this regime, the conditions $\lambda_n r_n^{\tau-1} \to \infty$ and $\lambda_n r_n^{\tau+1}/\mu_{n,\max} \to \infty$ are readily achievable. For instance, setting $\tau = 3$ and $\lambda_n = O(p^{1/4})$ suffices.

4.8.2 Choices of tuning parameters

In practice, $\mu_{n,\min}$ is estimated by $\hat{\mu}_{n,\min}$, the minimum eigenvalue of the sample instrument strength matrix [11]. We performed 5-fold data thinning to choose λ_n from a grid of values of the rate $(\hat{\mu}_{n,\min}/\sqrt{\hat{\mu}_{n,\min}+p})^{2/3}$ if $\hat{\mu}_{n,\min} > p$, or $(p/2)^{1/3}$ otherwise, and chose τ from (0.5, 1, 2, 3).

4.9 Simulation studies

We generated summary statistics by first simulating individual-level data. We considered K = 10 risk factors and p = 500 SNPs, with the correlation structure of SNP-exposure associations mimicking that in Figure 1c. Specifically, 20% of SNPs were associated with all risk factors, 40% with the first six, and the remaining 40% with the last four. True γ_{jk} values were drawn from mean-zero normal distributions and fixed across simulations.

Let $\Sigma_{\rho,K}$ denote a $K \times K$ compound symmetry matrix with diagonal entries equal to 1 and off-diagonal entries equal to ρ , where ρ controls the level of within-cluster correlations. Let $\mathbf{c}_{a \times b}$ be an $a \times b$ matrix of constant c. For SNPs associated with the first six risk factors,

$$(\gamma_{j1}, \dots, \gamma_{j6})^T \sim N(\mathbf{0}, \sigma_{\gamma}^2 \Sigma_{\text{cluster1}})$$
 and $(\gamma_7, \dots, \gamma_{j10})^T = \mathbf{0}$,

where

$$\Sigma_{ ext{cluster1}} = egin{bmatrix} \Sigma_{0.995,3} & \mathbf{0.5}_{3 imes 3} \ \mathbf{0.5}_{3 imes 3} & \Sigma_{0.9,3} \end{bmatrix}.$$

For SNPs associated with the last four risk factors,

$$(\gamma_{j1}, \dots, \gamma_{j6})^T = \mathbf{0}$$
 and $(\gamma_{j7}, \dots, \gamma_{j10})^T \sim N(\mathbf{0}, \sigma_{\gamma}^2 \Sigma_{\text{cluster 2}}),$

with $\Sigma_{\text{cluster2}} = \Sigma_{0.3,4}$. For SNPs associated with all ten risk factors,

$$(\gamma_{j1},\ldots,\gamma_{j10})^T \sim N(\mathbf{0},\sigma_{\gamma}^2\Sigma_{\text{all}}),$$

where

$$\Sigma_{
m all} = egin{bmatrix} \Sigma_{
m cluster1} & \mathbf{0.3}_{4 imes4} \ \mathbf{0.3}_{4 imes4} & \Sigma_{
m cluster2} \end{bmatrix}.$$

For each individual i = 1, ..., n, SNPs Z_{ij} were generated with minor allele frequencies MAF_j \sim Unif(0.01, 0.5). An unmeasured confounder $U_i \sim N(0, \sigma_u^2)$ was generated. The exposures X_{ik} 's and outcome Y_i were simulated as

$$X_{ik} = \mathbf{Z}_i^T \boldsymbol{\gamma}_k + U_i + e_{ik}, \quad k = 1, \dots, K,$$
$$Y_i = \mathbf{X}_i^T \boldsymbol{\beta}^* + U_i + E_i$$

where $\mathbf{Z}_i = (Z_{i1}, \dots, Z_{ip})^T$, $\mathbf{X}_i = s(X_{i1}, \dots, X_{iK})^T$ representing the standardized vector of exposures, $e_{ik} \sim N(0, \sigma_e^2)$, and $E_i \sim N(0, \sigma_e^2)$. We set $\sigma_{\gamma} = 0.001$, $\sigma_u = 2$ and $\sigma_e = 1$, corresponding to a many-weak-instruments setting with approximately 2% heritability across the risk factors.

This process was repeated to generate two independent datasets. Marginal SNP–exposure associations and their standard errors were obtained from simple linear regressions in one dataset, and SNP–outcome associations and their standard errors from regressions in the other. The true causal effects were set to $\beta^* = (1, 1, 1, 0, 0, 0, 0, 0, 0, 5, 0)$, with sample sizes $n = 1 \times 10^5$, 2×10^5 , and 3×10^5 .

We compared MVMR-PACS against alternative estimators listed in Table 1. IVW-LASSO was tuned by the 1SE rule. MR-BMA was implemented with a prior inclusion probability of 0.5 and default hyperparameters. For MVMR-cML-SuSiE, we first screened the ten risk factors using univariable MR-cML [40], then ran MVMR-cML-SuSiE initialized with the MVMR-cML [19] estimates for the selected factors. Risk factor selection was assessed by inclusion in any causal cluster (posterior inclusion probability greater than $1/K_s$, where K_s is the number of selected risk factors from the initial screening).

Data Availability

All data used in our study is in the public domain. Our study is based on publicly available summary-level data on genetic associations, which are referenced in Supplementary Table S5.

Code Availability

R code for MVMR-PACS is available at https://github.com/yinxiangwu/MVMR-PACS; R code for MR-BMA and IVW-Lasso is available at https://github.com/verena-zuber/demo_AMD; R code for MVMR-cML-SuSiE is available at https://github.com/lapsumchan/MVMR-cML-SuSiE; R code for SRIVW is available at https://github.com/tye27/mr.divw. R code for the simulation study and real data application is available at https://github.com/yinxiangwu/MVMR-PACS.

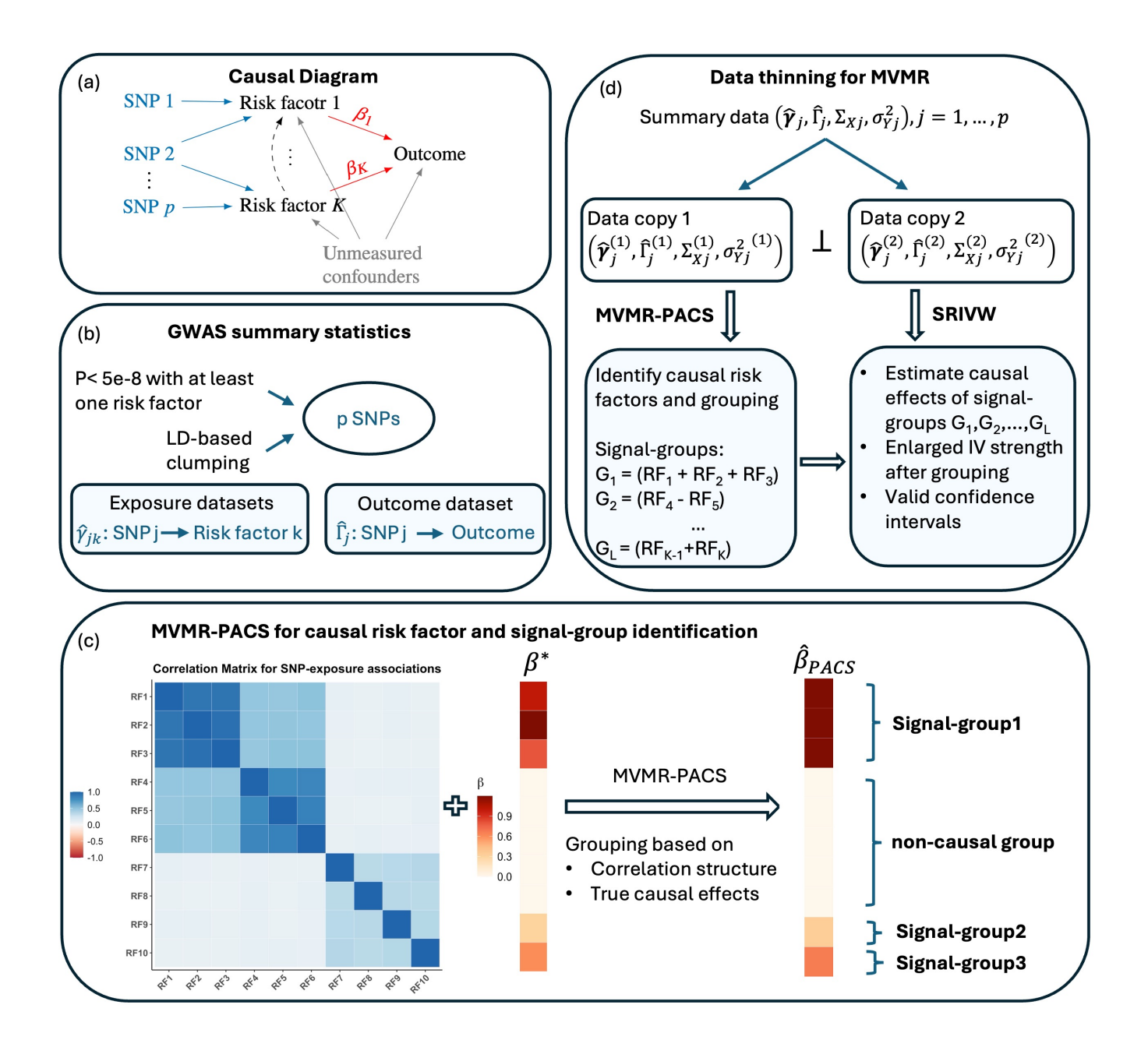


Figure 1: Overview of the MVMR-PACS framework for variable selection and post-selection inference. (a) We look for SNPs that satisfy the three core instrument assumptions: SNPs are conditionally associated with each exposure (relevance), are independent of unmeasured confounders (independence), and influence the outcome only through the included exposures (exclusion restriction). (b) Instruments are selected using a p-value threshold and LD clumping, based on GWAS summary statistics. (c) An illustrative example demonstrating the MVMR-PACS approach; MVMR-PACS identifies signal-groups of exposures, based on both correlation structure of observed SNP-exposure associations and true causal effects β^* . (d) Data thinning procedure for summary-data MVMR; observed summary statistics are split into two independent copies, enabling valid post-selection inference. RF: risk factor.

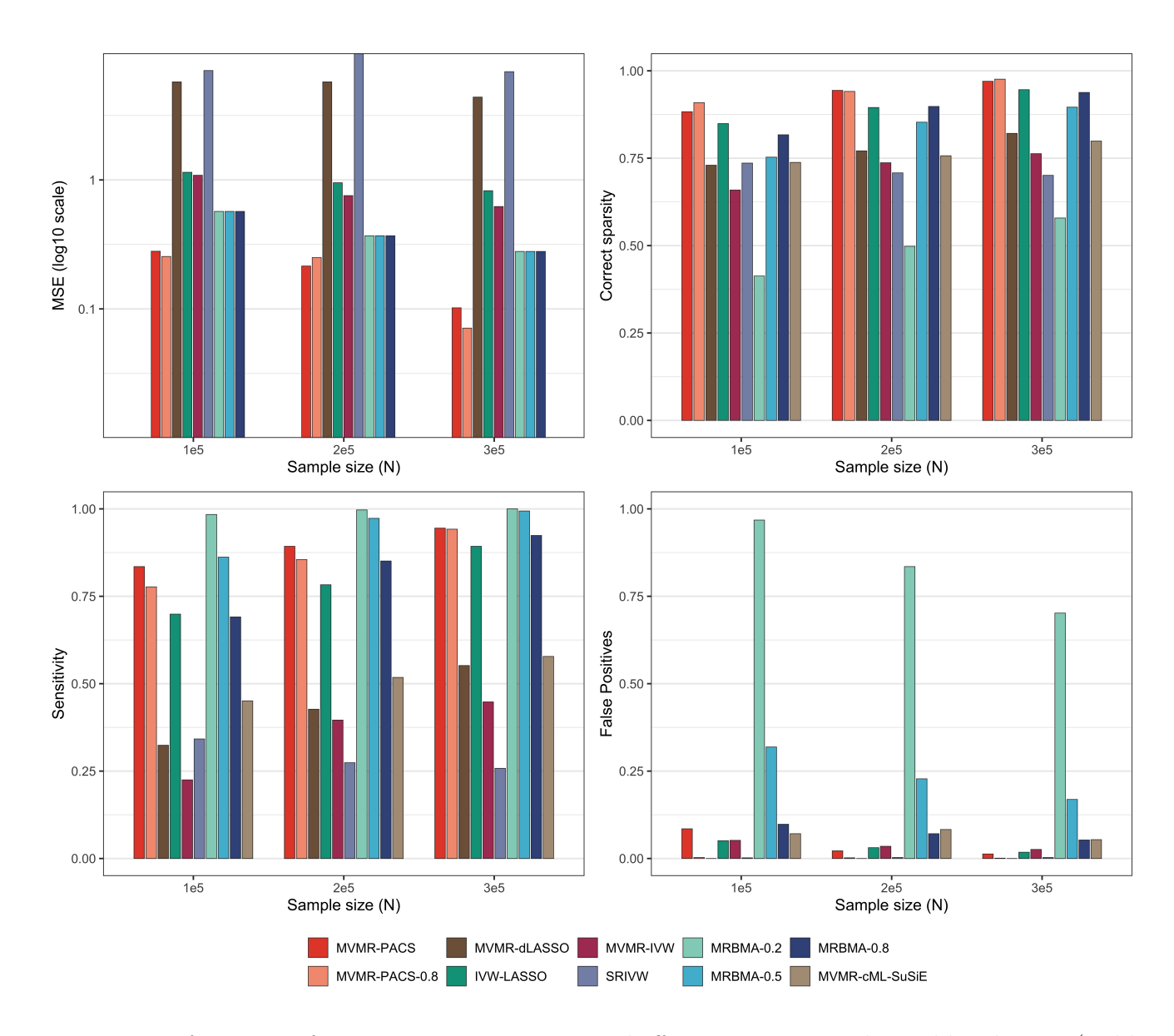


Figure 2: Performance of MVMR estimators in causal effect estimation and variable selection (Table 1). The figure summarizes results from simulations with sample sizes $N=1\times 10^5$, 2×10^5 , and 3×10^5 , reporting median mean squared error (MSE), correct sparsity, sensitivity, and false positive rate across 1,000 replicates. The average instrument strength parameters are -0.2, 1.9, and 4.0, for each sample size respectively. MVMR-PACS-0.8 is a variant of MVMR-PACS, incorporating a correlation threshold of 0.8 into its penalty. MR-BMA-0.2, MR-BMA-0.5, and MR-BMA-0.8 denote Bayesian model averaging with MIP thresholds of 0.2, 0.5, and 0.8; they all share the same model-averaged effect estimates and hence the same MSE estimates. MSE is not reported for MVMR-cML-SuSiE.

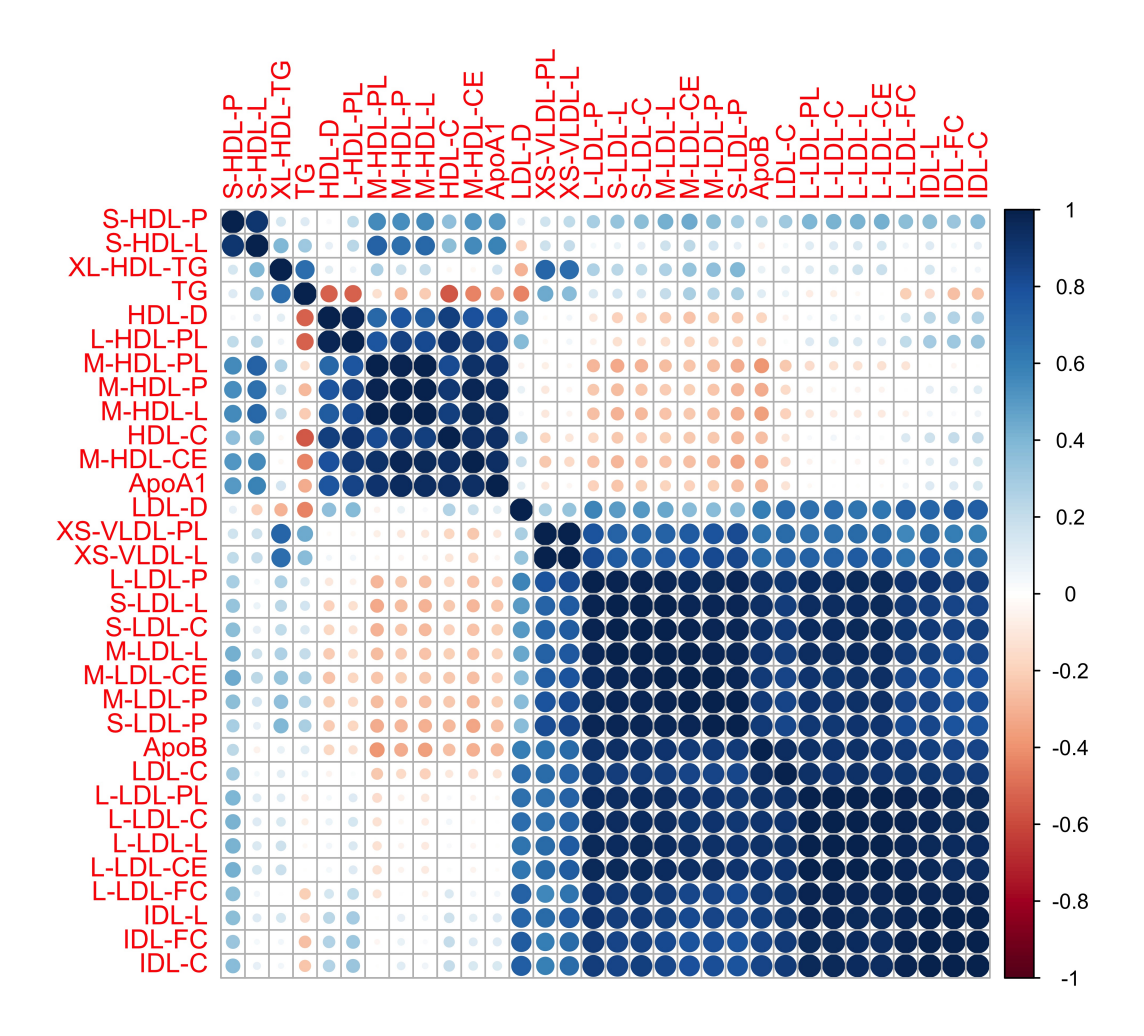


Figure 3: Correlations of SNP-exposure associations among 32 lipid traits based on 591 selected SNPs.

Table 2: Point estimates of individual traits across estimators. Estimates are shown on the log-odds scale. Values with absolute magnitude below 0.001 are denoted as "-". For MR-BMA, model-averaged effect estimates are reported.

Traits	IVW	SRIVW	IVW-LASSO	MVMR-dLASSO	MVMR-PACS	MR-BMA
XS-VLDL-PL	7.237	1.256	-	-	0.165	0.563
XS-VLDL-L	-5.663	-1.797	-	-	0.165	0.050
L-LDL-FC	7.825	-25.623	-	-	0.165	-0.014
$\operatorname{IDL-L}$	-9.148	-9.736	-	-	0.165	-0.308
IDL-FC	-1.217	-0.949	-	-	0.165	0.016
IDL-C	5.688	11.300	-	-	0.165	-0.392
LDL-D	-0.360	1.593	-	-	-0.165	-0.028
L-LDL-P	-2.084	-0.582	-	-	-0.351	-1.328
M-LDL-P	-1.198	1.671	-	-	-0.351	0.020
M-LDL-L	0.320	-10.824	-	-	-0.351	0.222
M-LDL-CE	1.534	3.154	-	-	-0.351	0.012
S-LDL-P	-0.780	0.690	-	-	-0.351	-0.803
S-LDL-L	-3.090	-0.501	-	-	-0.351	-0.051
S-LDL-C	0.586	6.723	-0.340	-1.911	-0.351	-0.510
L-HDL-PL	3.782	1.797	-	-	-0.049	1.137
M-HDL-PL	-1.859	-7.468	-	-	-0.049	-0.041
M-HDL-P	-2.633	3.198	-0.070	-	-0.049	-0.213
M-HDL-L	8.745	7.439	-	-	-0.049	-0.065
M-HDL-CE	-2.902	-5.299	-0.040	-	-0.049	0.012
HDL-D	-3.580	-1.731	-	-0.240	-0.314	-1.173
ApoB	-0.752	0.784	-	0.721	0.422	-0.497
LDL-C	1.307	0.637	0.732	1.301	1.218	1.201
TG	0.350	-0.392	0.117	0.188	0.362	0.408
L-LDL-PL	7.101	-0.181	-	-	-	0.134
L- LDL - L	2.143	8.681	-	-	-	0.661
L-LDL-C	-38.804	71.081	-	-	-	0.510
L-LDL-CE	30.783	-56.568	-	-	-	0.984
XL-HDL-TG	-0.107	-0.062	-	-	-	-0.009
S-HDL-P	0.443	-3.357	-0.030	-	-	-0.092
S-HDL-L	-4.019	3.812	-	-	-	-0.501
ApoA1	-0.263	1.634	-0.010	-	-	-0.167
HDL-C	-0.007	-0.409	-0.118			-0.003

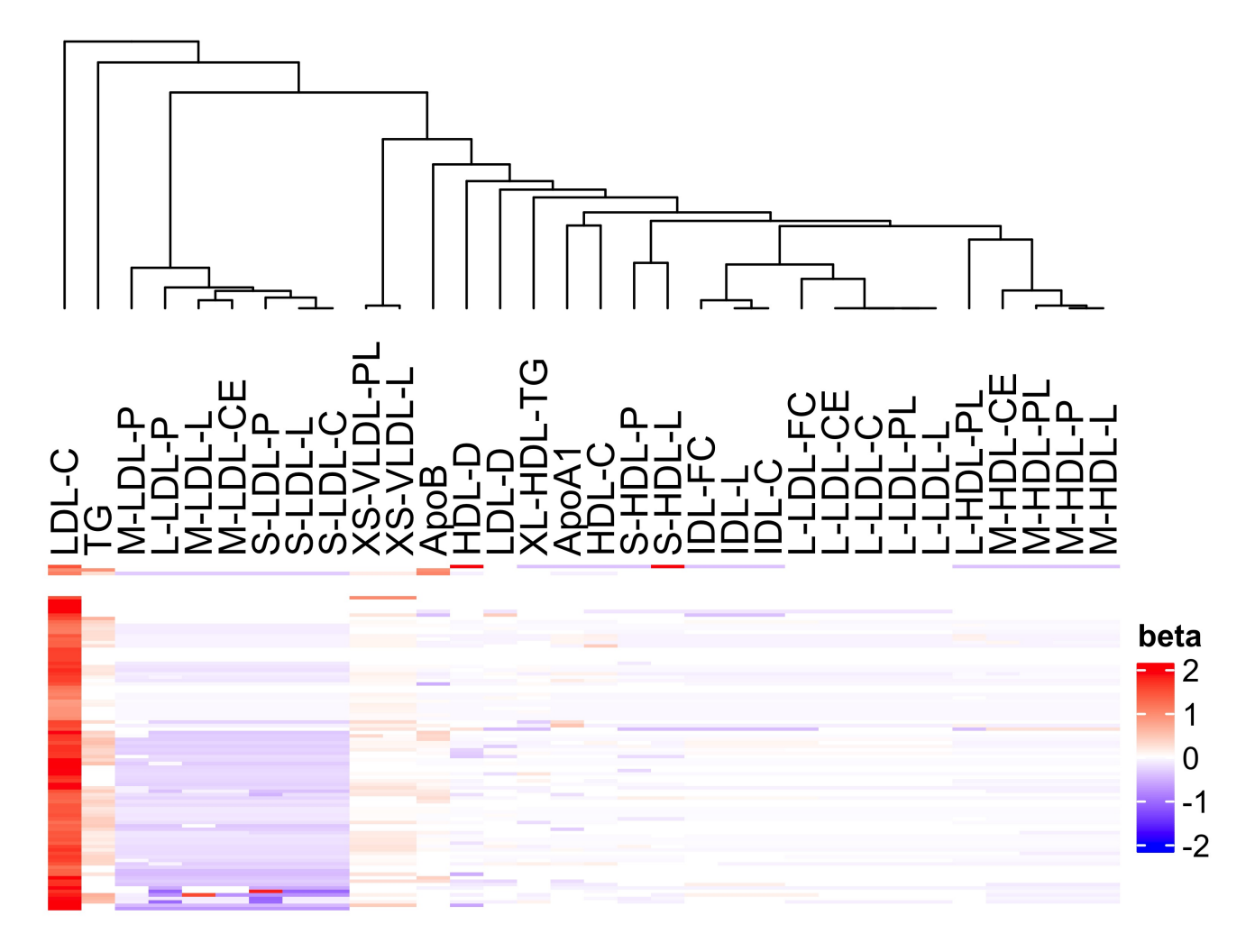


Figure 4: Heatmap of estimated causal effects across 100 data-thinning replicates. Shown are MVMR-PACS estimates (log-odds scale) for exposures that were nonzero and statistically significant at p < 0.05 in at least one replicate. Red indicates harmful effects and blue indicates protective effects on CAD risk. The dendrogram represents hierarchical clustering of the 32 traits based on their frequency of co-assignment to the same signal-group across replicates. Median [inter-quartile range] of instrument strength parameter [11] in the inference dataset is 14.8 [7.5, 49.8] across 100 data thinning replicates.

References

- [1] George Davey Smith and Shah Ebrahim. 'Mendelian randomization': can genetic epidemiology contribute to understanding environmental determinants of disease? *International Journal of Epidemiology*, 32(1):1–22, 2003.
- [2] Eleanor Sanderson, M Maria Glymour, Michael V Holmes, Hyunseung Kang, Jean Morrison, Marcus R Munafò, Tom Palmer, C Mary Schooling, Chris Wallace, Qingyuan Zhao, et al. Mendelian randomization. *Nature Reviews Methods Primers*, 2(1):6, 2022.
- [3] Eleanor Sanderson. Multivariable Mendelian randomization and mediation. Cold Spring Harbor Perspectives in Medicine, page a038984, 2020.
- [4] Rebecca C Richmond and George Davey Smith. Mendelian randomization: concepts and scope. Cold Spring Harbor Perspectives in Medicine, 12(1):a040501, 2022.
- [5] Marie C Sadler, Chiara Auwerx, Kaido Lepik, Eleonora Porcu, and Zoltán Kutalik. Quantifying the role of transcript levels in mediating dna methylation effects on complex traits and diseases. *Nature Communications*, 13(1):7559, 2022.
- [6] Yihao Lu, Ke Xu, Nathaniel Maydanchik, Bowei Kang, Brandon L Pierce, Fan Yang, and Lin S Chen. An integrative multi-context mendelian randomization method for identifying risk genes across human tissues. The American Journal of Human Genetics, 111(8):1736–1749, 2024.
- [7] Satoshi Yoshiji, Tianyuan Lu, Guillaume Butler-Laporte, Julia Carrasco-Zanini-Sanchez, Chen-Yang Su, Yiheng Chen, Kevin Liang, Julian Daniel Sunday Willett, Shidong Wang, Darin Adra, et al. Integrative proteogenomic analysis identifies col6a3-derived endotrophin as a mediator of the effect of obesity on coronary artery disease. *Nature Genetics*, pages 1–13, 2025.
- [8] Miguel A Hernán and James M Robins. Estimating causal effects from epidemiological data. Journal of Epidemiology & Community Health, 60(7):578–586, 2006.
- [9] Eleanor Sanderson, Wes Spiller, and Jack Bowden. Testing and correcting for weak and pleiotropic instruments in two-sample multivariable Mendelian randomization. *Statistics in Medicine*, 40(25):5434–5452, 2021.
- [10] Ashish Patel, James Lane, and Stephen Burgess. Weak instruments in multivariable Mendelian randomization: methods and practice. arXiv preprint arXiv:2408.09868, 2024.
- [11] Yinxiang Wu, Hyunseung Kang, and Ting Ye. A more robust approach to multivariable Mendelian randomization. *Biometrika*, page asaf053, 2025.

- [12] Qingyuan Zhao, Jingshu Wang, Zhen Miao, Nancy R Zhang, Sean Hennessy, Dylan S Small, and Daniel J Rader. A Mendelian randomization study of the role of lipoprotein subfractions in coronary artery disease. *eLife*, 10:e58361, 2021.
- [13] Lap Sum Chan, Mykhaylo M Malakhov, and Wei Pan. A novel multivariable Mendelian randomization framework to disentangle highly correlated exposures with application to metabolomics. *The American Journal of Human Genetics*, 2024.
- [14] Yi-Xuan Qiang, Yi-Xuan Wang, Xiao-Yu He, Yue-Ting Deng, Yi-Jun Ge, Bang-Sheng Wu, You Jia, Jian-Feng Feng, Wei Cheng, and Jin-Tai Yu. Genetic architecture of plasma metabolome in 254,825 individuals. *Nature Communications*, 16(1):8272, 2025.
- [15] Stephen Burgess and Simon G Thompson. Multivariable Mendelian randomization: the use of pleiotropic genetic variants to estimate causal effects. *American Journal of Epidemiology*, 181(4):251–260, 2015.
- [16] Jessica MB Rees, Angela M Wood, and Stephen Burgess. Extending the MR-Egger method for multivariable Mendelian randomization to correct for both measured and unmeasured pleiotropy. *Statistics in Medicine*, 36(29):4705–4718, 2017.
- [17] Andrew J Grant and Stephen Burgess. Pleiotropy robust methods for multivariable Mendelian randomization. *Statistics in Medicine*, 40(26):5813–5830, 2021.
- [18] Jingshu Wang, Qingyuan Zhao, Jack Bowden, Gibran Hemani, George Davey Smith, Dylan S. Small, and Nancy R. Zhang. Causal inference for heritable phenotypic risk factors using heterogeneous genetic instruments. *PLOS Genetics*, 17(6):1–24, 06 2021. doi: 10.1371/journal.pgen.1009575. URL https://doi.org/10.1371/journal.pgen.1009575.
- [19] Zhaotong Lin, Haoran Xue, and Wei Pan. Robust multivariable Mendelian randomization based on constrained maximum likelihood. *The American Journal of Human Genetics*, 110 (4):592–605, 2023.
- [20] Noah Lorincz-Comi, Yihe Yang, Gen Li, and Xiaofeng Zhu. MRBEE: A novel bias-corrected multivariable Mendelian randomization method. *bioRxiv*, pages 2023–01, 2023.
- [21] Verena Zuber, Johanna Maria Colijn, Caroline Klaver, and Stephen Burgess. Selecting likely causal risk factors from high-throughput experiments using multivariable Mendelian randomization. *Nature Communications*, 11(1):29, 2020.
- [22] Vasileios Karageorgiou, Dipender Gill, Jack Bowden, and Verena Zuber. Sparse dimensionality reduction approaches in Mendelian randomisation with highly correlated exposures. *Elife*, 12: e80063, 2023.

- [23] Chen Hao, Hou Lei, Xiaohua Zhou, and Fuzhong Xue. Transfer learning for Mendelian randomization with pleiotropic and correlated high-dimensional exposures and its application to trans-ethnic populations. 2025.
- [24] Dhruv B Sharma, Howard D Bondell, and Hao Helen Zhang. Consistent group identification and variable selection in regression with correlated predictors. *Journal of Computational and Graphical Statistics*, 22(2):319–340, 2013.
- [25] Anna Neufeld, Ameer Dharamshi, Lucy L Gao, and Daniela Witten. Data thinning for convolution-closed distributions. arXiv preprint arXiv:2301.07276, 2023.
- [26] Andrew J Grant and Stephen Burgess. An efficient and robust approach to Mendelian randomization with measured pleiotropic effects in a high-dimensional setting. *Biostatistics*, 23 (2):609–625, 2022.
- [27] Hongyu Zhao, Wei Jiang, Shuang Song, Liangbo Lyu, Changgee Chang, Yize Zhao, Baolin Wu, Lan Wang, and Matthew Girgenti. A robust penalized-regression-based method for multivariable Mendelian randomization using gwas summary statistics. 2023.
- [28] Samia Mora. Advanced lipoprotein testing and subfractionation are not (yet) ready for routine clinical use. *Circulation*, 119(17):2396–2404, 2009.
- [29] Emerging Risk Factors Collaboration et al. Lipid-related markers and cardiovascular disease prediction. *Jama*, 307(23):2499, 2012.
- [30] Abdolreza Chary, Maryam Tohidi, and Mehdi Hedayati. Association of Idl-cholesterol subfractions with cardiovascular disorders: A systematic review. *BMC Cardiovascular Disorders*, 23(1):533, 2023.
- [31] Patrick R Lawler, Akintunde O Akinkuolie, Paulo Harada, Robert J Glynn, Daniel I Chasman, Paul M Ridker, and Samia Mora. Residual risk of atherosclerotic cardiovascular events in relation to reductions in very-low-density lipoproteins. *Journal of the American Heart Association*, 6(12):e007402, 2017.
- [32] Allan D Sniderman, George Thanassoulis, Tamara Glavinovic, Ann Marie Navar, Michael Pencina, Alberico Catapano, and Brian A Ference. Apolipoprotein b particles and cardiovascular disease: a narrative review. *JAMA cardiology*, 4(12):1287–1295, 2019.
- [33] Ameer Dharamshi, Anna Neufeld, Keshav Motwani, Lucy L Gao, Daniela Witten, and Jacob Bien. Generalized data thinning using sufficient statistics. *Journal of the American Statistical Association*, 120(549):511–523, 2025.

- [34] Gibran Hemani, Jie Zheng, Benjamin Elsworth, Kaitlin H Wade, Valeriia Haberland, Denis Baird, Charles Laurin, Stephen Burgess, Jack Bowden, Ryan Langdon, Vanessa Y Tan, James Yarmolinsky, Hashem A Shihab, Nicholas J Timpson, David M Evans, Caroline Relton, Richard M Martin, George Davey Smith, Tom R Gaunt, Philip C Haycock, and Ruth Loos. The MR-Base platform supports systematic causal inference across the human phenome. *eLife*, 7:e34408, 2018.
- [35] Qingyuan Zhao, Jingshu Wang, Gibran Hemani, Jack Bowden, and Dylan S Small. Statistical inference in two-sample summary-data Mendelian randomization using robust adjusted profile score. *Annals of Statistics*, 48(3):1742–1769, 2020.
- [36] Brendan Bulik-Sullivan, Hilary K Finucane, Verneri Anttila, Alexander Gusev, Felix R Day, Po-Ru Loh, ReproGen Consortium, Psychiatric Genomics Consortium, Genetic Consortium for Anorexia Nervosa of the Wellcome Trust Case Control Consortium 3, Laramie Duncan, et al. An atlas of genetic correlations across human diseases and traits. *Nature Genetics*, 47 (11):1236–1241, 2015.
- [37] Marie Verbanck, Chia-Yen Chen, Benjamin Neale, and Ron Do. Detection of widespread horizontal pleiotropy in causal relationships inferred from Mendelian randomization between complex traits and diseases. *Nature Genetics*, 50(5):693–698, 2018.
- [38] Abhirup Datta and Hui Zou. Cocolasso for high-dimensional error-in-variables regression.

 Annals of Statistics, 2017.
- [39] Hui Zou. The adaptive lasso and its oracle properties. *Journal of the American statistical association*, 101(476):1418–1429, 2006.
- [40] Haoran Xue, Xiaotong Shen, and Wei Pan. Constrained maximum likelihood-based Mendelian randomization robust to both correlated and uncorrelated pleiotropic effects. *The American Journal of Human Genetics*, 108(7):1251–1269, 2021.
- [41] Tom G Richardson, Eleanor Sanderson, Tom M Palmer, Mika Ala-Korpela, Brian A Ference, George Davey Smith, and Michael V Holmes. Evaluating the relationship between circulating lipoprotein lipids and apolipoproteins with risk of coronary heart disease: a multivariable mendelian randomisation analysis. *PLoS medicine*, 17(3):e1003062, 2020.
- [42] Sarah E Graham, Shoa L Clarke, Kuan-Han H Wu, Stavroula Kanoni, Greg JM Zajac, Shweta Ramdas, Ida Surakka, Ioanna Ntalla, Sailaja Vedantam, Thomas W Winkler, et al. The power of genetic diversity in genome-wide association studies of lipids. *Nature*, 600(7890):675–679, 2021.
- [43] Tom G Richardson, Genevieve M Leyden, Qin Wang, Joshua A Bell, Benjamin Elsworth, George Davey Smith, and Michael V Holmes. Characterising metabolomic signatures of

- lipid-modifying therapies through drug target mendelian randomisation. *PLoS biology*, 20 (2):e3001547, 2022.
- [44] Christopher P Nelson, Anuj Goel, Adam S Butterworth, Stavroula Kanoni, Tom R Webb, Eirini Marouli, Lingyao Zeng, Ioanna Ntalla, Florence Y Lai, Jemma C Hopewell, et al. Association analyses based on false discovery rate implicate new loci for coronary artery disease. *Nature Genetics*, 49(9):1385–1391, 2017.
- [45] Howard D Bondell and Brian J Reich. Simultaneous regression shrinkage, variable selection, and supervised clustering of predictors with oscar. *Biometrics*, 64(1):115–123, 2008.
- [46] Daniela M Witten, Ali Shojaie, and Fan Zhang. The cluster elastic net for high-dimensional regression with unknown variable grouping. *Technometrics*, 56(1):112–122, 2014.
- [47] Gregor Buch, Andreas Schulz, Irene Schmidtmann, Konstantin Strauch, and Philipp S Wild. A systematic review and evaluation of statistical methods for group variable selection. *Statistics in Medicine*, 42(3):331–352, 2023.

Acknowledgments

T.Y.'s research was partially supported by the National Institute Of General Medical Sciences of the National Institutes of Health under Award Number R35GM155070.

Author Contributions

Y.W. and T.Y. conceived and designed the study. Y.W. performed the statistical analyses and theoretical development under the supervision of T.Y. N.M.D. contributed to the study design and interpretation of the results. Y.W. and T.Y. wrote the manuscript, and all authors reviewed and approved this version.

Corresponding Author

Correspondence to Ting Ye.

Supplement to "Group Identification and Variable Selection in Multivariable Mendelian Randomization with Highly-Correlated Exposures"

S1 Additional simulation details and results

Table S1: Numerical results from simulations with sample sizes $N=1\times 10^5$, 2×10^5 , and 3×10^5 , reporting median mean squared error (MSE), correct sparsity, sensitivity, and false positive rate across 1000 replicates. MVMR-PACS-0.8 is a variant of MVMR-PACS, incorporating a correlation threshold of 0.8 into its weighting scheme. MR-BMA-0.2, MR-BMA-0.5, and MR-BMA-0.8 denote Bayesian model averaging with MIP thresholds of 0.2, 0.5, and 0.8; they all share the same model-averaged effect estimates and hence the same MSE estimates. MSE is not reported for MVMR-cML-SuSiE and marked as "NA".

		MSE		Cor	rrect Spar	sity	;	Sensitivity	7	Fa	alse Positi	ve
Estimator	1×10^5	2×10^5	3×10^{5}	1×10^{5}	2×10^5	3×10^{5}	1×10^{5}	2×10^{5}	3×10^5	1×10^5	2×10^5	3×10^{5}
MVMR-IVW	1.087	0.756	0.622	0.659	0.737	0.763	0.225	0.396	0.448	0.052	0.035	0.026
SRIVW	7.047	9.585	6.905	0.736	0.708	0.701	0.342	0.274	0.258	0.002	0.003	0.003
IVW-LASSO	1.146	0.951	0.825	0.849	0.895	0.946	0.699	0.783	0.893	0.051	0.031	0.018
MVMR-dLASSO	5.757	5.759	4.387	0.73	0.771	0.821	0.324	0.427	0.552	0.000	0.000	0.000
MVMR-PACS	0.28	0.215	0.102	0.883	0.944	0.97	0.835	0.893	0.945	0.085	0.022	0.013
MVMR-PACS-0.8	0.255	0.25	0.071	0.909	0.941	0.976	0.777	0.855	0.942	0.003	0.002	0.001
MRBMA-0.2	0.57	0.369	0.279	0.413	0.498	0.579	0.984	0.997	1.000	0.968	0.835	0.702
MRBMA-0.5	0.57	0.369	0.279	0.753	0.853	0.896	0.862	0.973	0.994	0.319	0.228	0.169
MRBMA-0.8	0.57	0.369	0.279	0.817	0.898	0.938	0.691	0.851	0.924	0.098	0.071	0.053
MVMR-cML-SuSiE	NA	NA	NA	0.738	0.757	0.799	0.451	0.518	0.578	0.071	0.083	0.054

S1.1 Graphical results

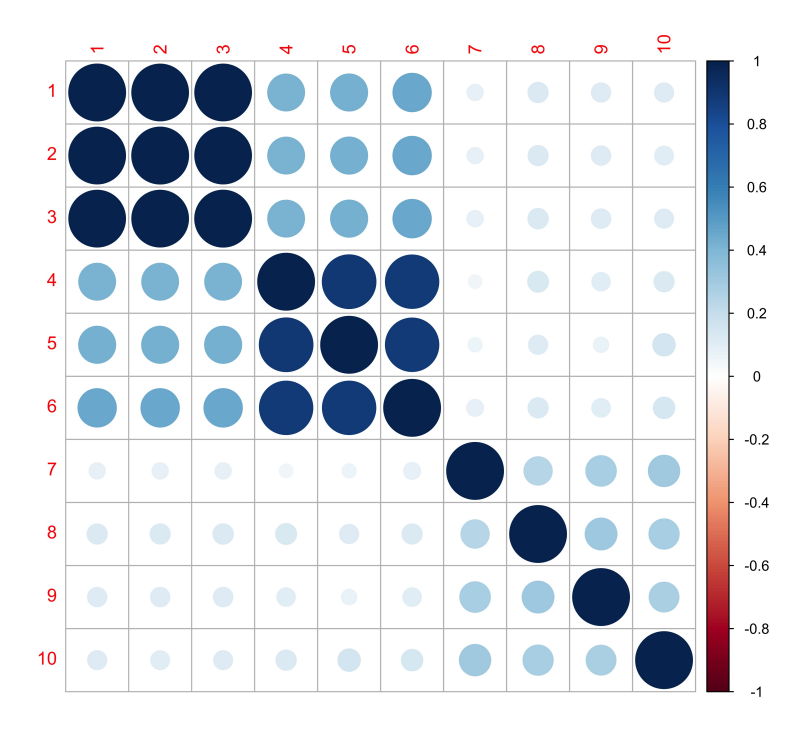


Figure S1: The correlation matrix of true SNP-exposure associations across 500 SNPs.

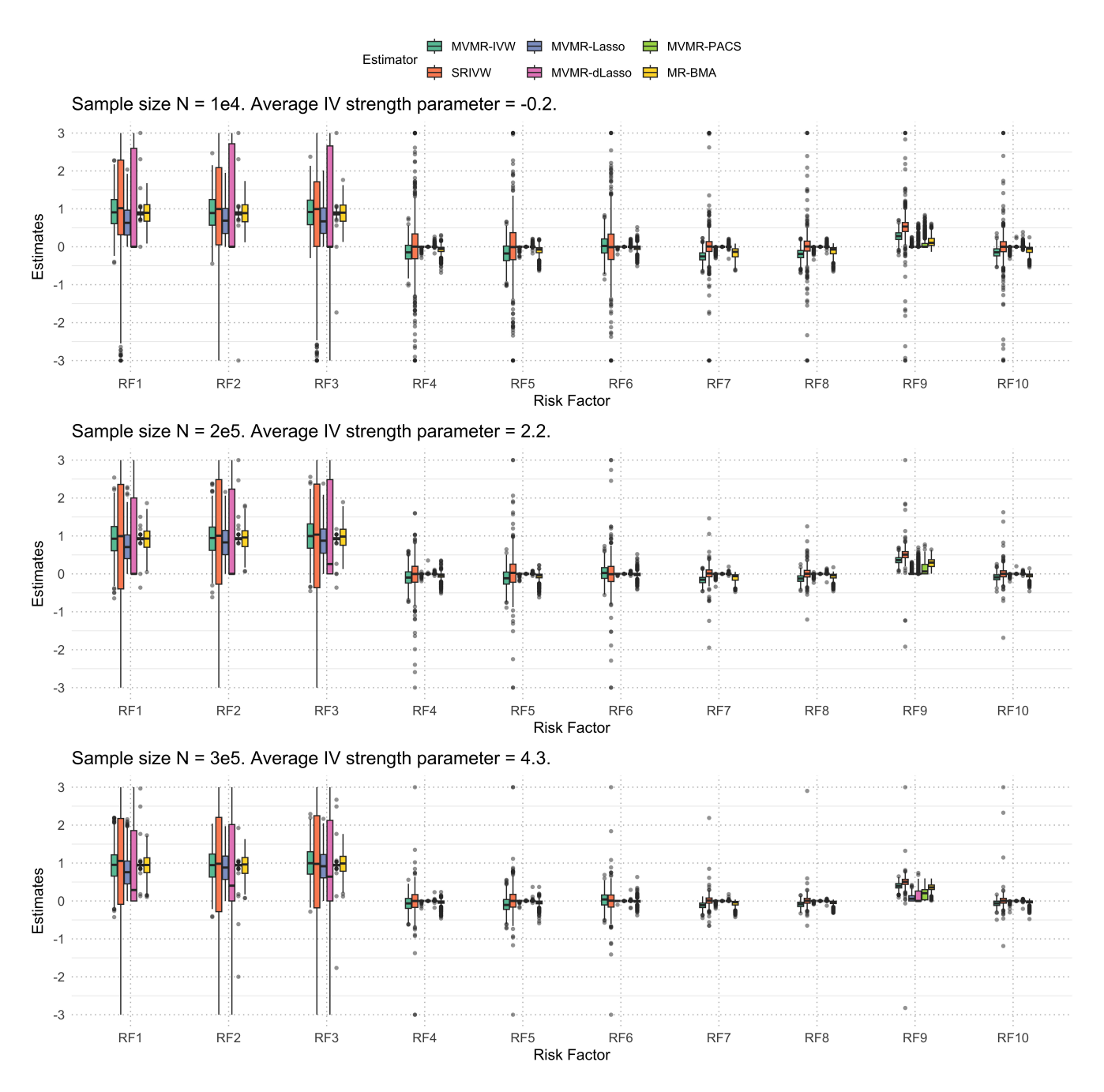


Figure S2: Boxplots of point estimates from different estimators across different exposures and sample sizes. Y-axis is cupped between -3 and 3 for better visibility. Abbreviations: RF: risk factor.

S1.2 Post-selection inference results

Sample size	instrument strength	Correct Sparsity	Sensitivity	False Positive
1e5	44.5	0.834	0.823	0.158
2e5	86.7	0.910	0.850	0.050
3e5	124.6	0.923	0.871	0.042

Table S2: MVMR-PACS performance in the selection dataset generated through data thinning. Sample size refers to the sample size of the individual-level data that are used to generate summary statistics. The instrument strength column reports the mean instrument strength parameter based on grouped exposures in the selection dataset. Data generating process is the same as in the simulation study.

Sample size	1-1-1-0-0-0-0-0-0	1-1-1-0-0-0-0-0-2-0	other
1e5	77.5%	13.2%	9.3%
2e5	61.5%	34.2%	4.3%
3e5	55.3%	44.2%	2.5%

Table S3: Frequency of different groupings selected by MVMR-PACS in the training dataset generated through two-fold data thinning over 1000 simulation runs. The header of the table includes four typical groupings. Risk factors assigned with the same number form a signal-group, and a risk factor is labelled 0 if it is selected as non-causal. For example, 1-1-1-0-0-0-0-0-0 means the first three risk factors are selected as a signal-group, while the remaining risk factors are selected as non-causal. Grouping 1-1-1-0-0-0-0-0-2-0 corresponds to the true model.

Sample size	Signal-group 1	Signal-group 2
1e5 2e5	0.949 0.950	0.950 0.940
3e5	0.939	0.941

Table S4: Coverage probabilities of 95% confidence intervals constructed by SRIVW based on the inferential dataset when the model is correctly identified. Signal-group 1 is the group of risk factors 1 to 3. Signal-group 2 includes only risk factor 9.

S2Additional real data application details

S2.1Data sources

Table S5: Data sources for exposures and outcome.

Phenotype	Sample size	Ancestry	Source	Reference	Download link
Apolipoprotein A-I	393,193	European	UK Biobank	[41]	https:// opengwas. io/datasets/ ieu-b-107
Apolipoprotein B	439,214	European	UK Biobank	[41]	https:// opengwas. io/datasets/ ieu-b-108
LDL-C	$1.32\mathrm{M}$	European	GLGC	[42]	https://csg. sph.umich.edu/ willer/public/ glgc-lipids2021/
HDL-C	$1.32\mathrm{M}$	European	GLGC	[42]	https://csg. sph.umich.edu/ willer/public/ glgc-lipids2021/
TG	$1.32\mathrm{M}$	European	GLGC	[42]	https://csg. sph.umich.edu/ willer/public/ glgc-lipids2021/
Lipoprotein sub- fraction traits	115,082	European	UK Biobank	[43]	https://www. ebi.ac.uk/gwas/ publications/ 35213538
Coronary artery disease		Mostly European	CARDIoGRA plusC4D + UK Biobank	M[44]	https://www. ebi.ac.uk/gwas/ publications/ 35213538

S2.2 MR-BMA posterior inclusion probability

Table S6: MR-BMA results: marginal inclusion probabilities and average effects.

trait	marginal inclusion	average effect
LDL-C	1.000	1.202
TG	0.996	0.408
ApoB	0.989	-0.497
L-LDL-P	0.988	-1.330
HDL-D	0.975	-1.173
L-HDL-PL	0.967	1.141
L-LDL-CE	0.896	0.996
S-LDL-P	0.882	-0.788
XS-VLDL-PL	0.849	0.544
S-HDL-L	0.745	-0.499
L-LDL-L	0.737	0.648
S-LDL-C	0.673	-0.525
L-LDL-C	0.652	0.496
ApoA1	0.649	-0.166
IDL-C	0.647	-0.392
IDL-L	0.558	-0.295
M-LDL-L	0.498	0.236
M-HDL-P	0.461	-0.214
L-LDL-PL	0.434	0.134
XS-VLDL-L	0.415	0.063
L-LDL-FC	0.363	-0.016
M-HDL-L	0.360	-0.069
S-HDL-P	0.342	-0.090
S-LDL-L	0.315	-0.052
M-LDL-CE	0.314	0.013
M-HDL-PL	0.313	-0.044
M-HDL-CE	0.281	0.012
IDL-FC	0.227	0.014
M-LDL-P	0.191	0.018
LDL-D	0.124	-0.024
XL-HDL-TG	0.087	-0.009
HDL-C	0.071	-0.003

Table S7: Results from MVMR-cML analysis

Model	Exposure	Estimated effect
LDL-C, ApoA1, L-LDL-FC	LDL-C	2.084
	ApoA1	0.217
	L-LDL-FC	-2.037
LDL-C, ApoA1, IDL-L	LDL-C	2.355
	ApoA1	0.238
	IDL-L	-2.375
LDL-C, ApoA1, IDL-FC	LDL-C	1.592
	ApoA1	0.062
	IDL-FC	-1.451
LDL-C, ApoA1, IDL-C	LDL-C	1.519
	ApoA1	0.086
	IDL-C	-1.325
LDL-C, HDL-C, L-LDL-FC	LDL-C	2.759
	HDL-C	0.481
	L-LDL-FC	-3.014
LDL-C, HDL-C, IDL-L	LDL-C	2.574
	HDL-C	0.320
	IDL-L	-2.633
LDL-C, HDL-C, IDL-FC	LDL-C	2.244
	HDL-C	0.315
	IDL-FC	-2.271
LDL-C, HDL-C, IDL-C	LDL-C	2.138
	HDL-C	0.329
	IDL-C	-2.162

S3 Review of penalized regression methods for correlated data and clustered regression coefficients

When the columns of $\hat{\Pi}$ are highly correlated, ordinary weighted least squares estimates of $\boldsymbol{\beta}$ tend to be unstable. Penalized regression methods address this issue by introducing regularization to stabilize estimation.

In this section, we review commonly used penalized regression methods for estimating β^* in the linear model:

$$\hat{\mathbf{\Gamma}} = \hat{\Pi} \boldsymbol{\beta}^* + \boldsymbol{\epsilon} \tag{S1}$$

where $\boldsymbol{\epsilon} = (\epsilon_1, \dots, \epsilon_p)^T$, and $\epsilon_j \sim N(0, \sigma_{Y_j}^2)$ for every j. For simplicity, we assume that $\hat{\Pi}$ is

measured with negligible error, though we will relax this assumption in our proposed method.

These methods typically solve the following optimization problem:

$$\mathcal{L}(\boldsymbol{\beta}, \lambda) = \frac{1}{2} (\hat{\boldsymbol{\Gamma}} - \hat{\boldsymbol{\Pi}} \boldsymbol{\beta})^T W (\hat{\boldsymbol{\Gamma}} - \hat{\boldsymbol{\Pi}} \boldsymbol{\beta}) + \Omega(\boldsymbol{\beta}, \lambda)$$

where $W = \operatorname{diag}(\sigma_{Y_1}^{-2}, ..., \sigma_{Y_p}^{-2})$ accounts for heteroskedastic errors, and $\Omega(\boldsymbol{\beta}, \lambda)$ is a penalty function of $\boldsymbol{\beta}$ and tuning parameter λ . Well-known examples include LASSO with $\Omega(\boldsymbol{\beta}, \lambda) = \lambda ||\boldsymbol{\beta}||_1$, Ridge with $\Omega(\boldsymbol{\beta}, \lambda) = \lambda ||\boldsymbol{\beta}||_2$ and Elastic Net with $\Omega(\boldsymbol{\beta}, \lambda) = \lambda(\alpha ||\boldsymbol{\beta}||_1 + (1 - \alpha)||\boldsymbol{\beta}||_2^2)$, where α can be another tuning parameter or user-specified. To incorporate group structure among exposures, the sparse group LASSO adds an additional group-wise l_2 penalty: $\Omega(\boldsymbol{\beta}, \lambda) = \lambda(\alpha ||\boldsymbol{\beta}||_1 + (1 - \alpha)\sum_{l=1}^L ||\boldsymbol{\beta}_l||_2)$ where $\boldsymbol{\beta}_l$ is a vector of coefficients for the l-th group and α balances the sparsity between and within groups. However, when group structure is unknown, methods that can perform estimation and grouping simultaneously in a data-driven way are more practical.

To address this limitation, [24] proposed the pairwise absolute clustering and shrinkage (PACS) estimator with:

$$\Omega(\boldsymbol{\beta}, \lambda) = \lambda \left\{ \sum_{k=K} w_k |\beta_k| + \sum_{1 \le k < m \le K} w_{km(-)} |\beta_k - \beta_m| + \sum_{1 \le k < m \le K} w_{km(+)} |\beta_k + \beta_m| \right\}$$
 (S2)

where w_k , $w_{km(-)}$, and $w_{km(+)}$ are weights that can be user-specified or data-adaptive. For example, the weights are often based on correlations between columns of $\hat{\Pi}$. This penalty encourages both sparsity and grouping of effects of similar magnitude, without requiring pre-specified groups, a feature that is particularly appealing when highly correlated exposures have indistinguishable effects, as it tends to shrink them to a shared value.

Other related approaches include OSCAR [45] and the cluster elastic net (CEN) estimator [46]. The former can be considered as a special case of PACS [24]. CEN uses an l_1 penalty together with an l_2 within-cluster shrinkage penalty, and combines a data-driven clustering step via K-means. Unlike PACS, CEN encourages similarity within clusters but does not enforce exact equality of effects, and it requires the number of clusters to be pre-specified. Refer to [47] for a more comprehensive review of related approaches.

In this work, we adopt the PACS penalty for its ability to identify signal-groups—groups of risk factors with indistinguishable effects—without relying on prior group information.

S4 Estimand based on signal-groups

As noted in Methods Section 4.8, MVMR-PACS defines a transformation matrix G, which converts Π to a new design matrix $\Pi_g = \Pi G^T$ with L columns by collapsing elements of γ_j , i.e., summing those with nonzero effects of the same magnitude, subtracting those with opposite effects, and omitting those with zero effects. , where L is the number of identified groups. Based on this new design matrix for signal-groups, a working model is given by $\Gamma = \Pi_g C_g \beta^*$, where $\beta^* = (\beta_1^*, ..., \beta_L^*)$ represents the direct causal effects of L signal-groups. The estimand of interest based on the

working model is then

$$\boldsymbol{\beta}_q^* = (\boldsymbol{\Pi}_q^T W \boldsymbol{\Pi}_g)^{-1} \boldsymbol{\Pi}_q^T W \boldsymbol{\Gamma},$$

where $W = \operatorname{diag}(\sigma_{Y1}^{-2}, \dots, \sigma_{Yp}^{-2}).$

To demonstrate when this estimand is reasonable to pursue, we consider an example with $K_1 + K_2$ exposures where $K_1, K_2 > 1$.

Suppose that $\gamma_j = (\gamma_{j1}, \dots, \gamma_{jK_1}, \gamma_{j(K_1+1)}, \dots, \gamma_{j(K_1+K_2)})^T \sim N(\mathbf{0}, \Sigma_{\gamma})$, where Σ_{γ} is a well-defined positive definite matrix. Let ρ_{kl} denote the correlation coefficient for the correlation between γ_{jk} and γ_{jl} . $\Gamma_j = \gamma_j \boldsymbol{\beta}^* = \sum_{k=1}^{K_1} \gamma_{jk} \beta_k^* + \sum_{k=K_1+1}^{K_2} \gamma_{jk} \beta_k^*$. For simplicity, assume $\sigma_{Y_j}^2$'s are the same across j, all $\rho_{kl} \geq 0$, and diagonal terms of Σ_{γ} are all 1. For ease of notation, we omit the superscript * from all betas in the following derivations.

Let $g_{1j} = \sum_{k=1}^{K_1} \gamma_{jk}$ be the SNP-exposure association for the sum of first K_1 exposures (signal-group 1), and $g_{2j} = \sum_{k=K_1+1}^{K_2} \gamma_{jk}$ be the SNP-exposure association for the sum of remaining K_2 exposures (signal-group 2). Then, the working model based on the grouped exposures is

$$\Gamma_j = g_{1j}\tau_1 + g_{2j}\tau_2 + \epsilon_j$$

where ϵ_j measures the difference between the working model and the true model, which is likely correlated with g_{1j} and g_{2j} . Because of such correlation, when regressing Γ_j on g_{1j} and g_{2j} , τ_1 and τ_2 will generally be biased for β 's.

Our goal here is to compare τ_1 , τ_2 with original β 's, and discuss under which situation grouping may help.

First, we derive the formula for τ_1 and τ_2 . Note that

$$\begin{bmatrix} \tau_1 \\ \tau_2 \end{bmatrix} = (\Pi_g^T \Pi_g)^{-1} \Pi_g^T \Gamma$$
 where $\Pi_g = \Pi G^T$ with $G^T = \begin{bmatrix} \mathbf{1}_{K_1} & 0 \\ 0 & \mathbf{1}_{K2} \end{bmatrix}$, and
$$\Pi_g^T \Pi_g = \begin{bmatrix} \sum_j g_{1j}^2 & \sum_j g_{1j}g_{2j} \\ \sum_j g_{1j}g_{2j} & \sum_j g_{2j}^2 \end{bmatrix}$$

and

$$\Pi_g^T \Gamma = \begin{bmatrix} \sum_j g_{1j} \Gamma_j \\ \sum_j g_{2j} \Gamma_j \end{bmatrix}$$

As p is large, we have

$$\sum_{j} g_{1j}^{2} = p \operatorname{var}(g_{1j}) = p[K_{1} + 2 \sum_{k < l}^{K_{1}} \rho_{kl}] = p[K_{1} + C_{1}]$$

$$\sum_{j} g_{1j}g_{2j} = p\operatorname{cov}(g_{1j}, g_{2j}) = p\sum_{k=1}^{K_1} \sum_{l=K_1+1}^{K_1+K_2} \rho_{kl} = pD$$

$$\sum_{j} g_{2j}^{2} = p \operatorname{var}(g_{2j}) = p[K_{2} + 2 \sum_{K_{1} < k < l < K_{1} + K_{2}}^{K_{1} + K_{2}} \rho_{kl}] = p[K_{2} + C_{2}]$$

$$\sum_{j} g_{1j} \Gamma_{j} = p \operatorname{cov}(g_{1j}, \Gamma_{j}) = p \operatorname{cov}(\sum_{k=1}^{K_{1}} \gamma_{jk}, \sum_{k=1}^{K_{1}} \gamma_{jk} \beta_{k} + \sum_{k=K_{1}+1}^{K_{2}} \gamma_{jk} \beta_{k})$$

$$= p \left(\sum_{k=1}^{K_{1}} \beta_{k} + 2 \sum_{k< l}^{K_{1}} \rho_{kl} \beta_{l} + \sum_{k=1}^{K_{1}} \sum_{l=K_{1}+1}^{K_{1} + K_{2}} \rho_{kl} \beta_{l}\right) = p[K1\bar{\beta}_{1} + A_{1} + B_{1}]$$

$$\sum_{j} g_{2j} \Gamma_{j} = p \operatorname{cov}(g_{2j}, \Gamma_{j}) = p \operatorname{cov}(\sum_{k=K_{1}+1}^{K_{1} + K_{2}} \gamma_{jk}, \sum_{k=1}^{K_{1}} \gamma_{jk} \beta_{k} + \sum_{k=K_{1}+1}^{K_{2}} \gamma_{jk} \beta_{k})$$

$$=p\bigg(\sum_{k=K_1+1}^{K_1+K_2}\beta_k+2\sum_{K_1< k< l\leq K_1+K_2}^{K_1+K_2}\rho_{kl}\beta_l+\sum_{k=1}^{K_1}\sum_{l=K_1+1}^{K_1+K_2}\rho_{kl}\beta_k\bigg)=p[K_2\bar{\beta}_2+A_2+B_2]$$

where $\bar{\beta}_1 = \frac{1}{K_1} \sum_{k=1}^{K_1} \beta_k$ and $\bar{\beta}_2 = \frac{1}{K_2} \sum_{k=K_1+1}^{K_1+K_2} \beta_k$. Thus

$$\Pi_g^T \Pi_g \approx \begin{bmatrix} p \operatorname{var}(g_{1j}) & p \operatorname{cov}(g_{1j}, g_{2j}) \\ p \operatorname{cov}(g_{1j}, g_{2j}) & p \operatorname{var}(g_{2j}) \end{bmatrix}$$

$$(\Pi_g^T \Pi_g)^{-1} = \frac{1}{p(\operatorname{var}(g_{1j})\operatorname{var}(g_{2j}) - \operatorname{cov}(g_{1j}, g_{2j})^2)} \begin{bmatrix} \operatorname{var}(g_{2j}) & -\operatorname{cov}(g_{1j}, g_{2j}) \\ -\operatorname{cov}(g_{1j}, g_{2j}) & \operatorname{var}(g_{1j}) \end{bmatrix}$$

$$\Pi_g^T \Gamma \approx \begin{bmatrix} p \operatorname{cov}(g_{1j}, \Gamma_j) \\ p \operatorname{cov}(g_{2j}, \Gamma_j) \end{bmatrix}$$

Therefore, we have

$$\tau_{1} = \frac{\operatorname{var}(g_{2j})\operatorname{cov}(g_{1j}, \Gamma_{j}) - \operatorname{cov}(g_{1j}, g_{2j})\operatorname{cov}(g_{2j}, \Gamma_{j})}{\operatorname{var}(g_{1j})\operatorname{var}(g_{2j}) - \operatorname{cov}(g_{1j}, g_{2j})^{2}}$$
$$= \frac{(K_{2} + C_{2})(K_{1}\bar{\beta}_{1} + A_{1} + B_{1}) - D(K_{2}\bar{\beta}_{2} + A_{2} + B_{2})}{(K_{1} + C_{1})(K_{2} + C_{2}) - D^{2}}$$

and

$$\tau_{2} = \frac{\operatorname{var}(g_{1j})\operatorname{cov}(g_{2j}, \Gamma_{j}) - \operatorname{cov}(g_{1j}, g_{2j})\operatorname{cov}(g_{1j}, \Gamma_{j})}{\operatorname{var}(g_{1j})\operatorname{var}(g_{2j}) - \operatorname{cov}(g_{1j}, g_{2j})^{2}}$$

$$= \frac{(K_{1} + C_{1})(K_{2}\bar{\beta}_{2} + A_{2} + B_{2}) - D(K_{1}\bar{\beta}_{1} + A_{1} + B_{1})}{(K_{1} + C_{1})(K_{2} + C_{2}) - D^{2}}$$

Without further assumptions on β 's and ρ 's, we can see that each group's effect is a linear combination of all β 's in its own group and, through the correlation between the two groups, also dependent on the β 's in the other group.

However, there are certainly a few special settings where grouping can be beneficial.

Setting 1: β 's in a group are all equal.

Suppose $\beta_k = \alpha_1^*$ for all $k = 1, ..., K_1$ and $\beta_k = \alpha_2^*$ for all $k = K_1 + 1, ..., K_1 + K_2$. Then, $\bar{\beta}_1 = \alpha_1^*$, $A_1 = C_1\alpha_1^*$, $B_1 = D\alpha_2^*$, $\bar{\beta}_2 = \alpha_2^*$, $A_2 = C_2\alpha_2^*$, $B_2 = D\alpha_1^*$. Then, we have

$$\tau_{1} = \frac{(K_{2} + C_{2})(K_{1}\bar{\beta}_{1} + A_{1} + B_{1}) - D(K_{2}\bar{\beta}_{2} + A_{2} + B_{2})}{(K_{1} + C_{1})(K_{2} + C_{2}) - D^{2}}$$

$$= \frac{(K_{2} + C_{2})(K_{1}\alpha_{1}^{*} + C_{1}\alpha_{1}^{*} + D\alpha_{2}^{*}) - D(K_{2}\alpha_{2}^{*} + C_{2}\alpha_{2}^{*} + D\alpha_{1}^{*})}{(K_{1} + C_{1})(K_{2} + C_{2}) - D^{2}}$$

$$= \alpha_{1}^{*}$$

Similary, $\tau_2 = \alpha_2^*$. Hence, if the effects of risk factors that we intend to group are indeed equal, then we can still unbiasedly estimate that shared effects.

Setting 2: correlations within the two signal-groups are close to 1 and correlations between the two groups are identical, equal to r^* . Then, $A_1 = (K_1 - 1) \sum_{k=1}^{K_1} \beta_k = K_1^2 \bar{\beta}_1 - K_1 \bar{\beta}_1$, $B_1 = r^* K_1 K_2 \bar{\beta}_2$, $C_1 = K_1 (K_1 - 1)$, $A_2 = (K_2 - 1) \sum_{k=K_1+1}^{K_1+K_2} \beta_k = K_2^2 \bar{\beta}_2 - K_2 \bar{\beta}_2$, $B_2 = r^* K_1 K_2 \bar{\beta}_1$, $C_2 = K_2 (K_2 - 1)$, $D = r^* K_1 K_2$. Thus,

$$\tau_1 = \frac{K_2^2 (K_1^2 \bar{\beta}_1 + r^* K_1 K_2 \bar{\beta}_2) - r^* K_1 K_2 (K_2^2 \bar{\beta}_2 + r^* K_1 K_2 \bar{\beta}_1)}{K_1^2 K_2^2 - r^{*2} K_1^2 K_2^2}$$
$$= \bar{\beta}_1$$

Similarly, we can show $\tau_2 = \bar{\beta}_2$. Hence, when internal correlations are high, the direct causal effect of a signal-group would approximate an average of the causal effects of its group members.

Setting 3: correlations between the two signal-groups are equal to 0, i.e., $\rho_{kl} = 0$ for $k \in \{1, \ldots, K_1\}$ and $l \in \{K_1 + 1, \ldots, K_1 + K_2\}$. Then, $B_1 = B_2 = 0$ and D = 0.

$$\tau_1 = \frac{K_1 \bar{\beta}_1 + A_1}{K_1 + C_1}$$

$$= \frac{\sum_{k=1}^{K_1} \beta_k + 2 \sum_{k

$$K_2 \bar{\beta}_2 + A_2$$$$

$$\tau_2 = \frac{K_2 \bar{\beta}_2 + A_2}{K_2 + C_2}$$

$$= \frac{\sum_{k=K_1+1}^{K_1+K_2} \beta_k + 2\sum_{K_1 < k < l \le K_1+K_2}^{K_1+K_2} \rho_{kl} \beta_l}{K_2 + 2\sum_{K_1 < k < l \le K_1+K_2}^{K_1+K_2} \rho_{kl}}$$

Hence, when the correlations across signal-groups are close to 0, the direct causal effect of a signal-group would approximate a weighted average of the causal effects of its group members.

In the above derivations, we assume that diagonal terms of Σ_{γ} are all 1. If this is not the case, then above derivations still go through, but the formula becomes more complicated. In particular, in setting 2 where internal correlations are high, the direct causal effect of a signal-group is no longer a simple average of the causal effects of its group members. Instead, it becomes a weighted

average of the causal effects of its group members, with weights depending on the variance of γ_j . We also assume that all $\rho_{kl} \geq 0$. If $\rho_{kl} \to -1$, MVMR-PACS would tend to create a signal-group with the contrast between exposure k and l. In this case, we can take the difference between the two exposures and conduct a similar analysis.

S5 MVMR-PACS-x estimator

MVMR-PACS-x additionally incorporates a correlation threshold of value x, e.g., 0.8, into its weighting scheme. Specifically, the weights $w_{km(-)}$ and $w_{km(+)}$ in MVMR-PACS are further multiplier by indicator functions $I(\hat{r}_{km} > r^*)$ and $I(\hat{r}_{km} < -r^*)$, respectively. In other words, $w_{km(-)}$ and $w_{km(+)}$ are non-zero, only when the observed correlations exceed a pre-specified threshold r^* , e.g., $r^* = 0.8$. When all observed correlations fall below this threshold in magnitude, the PACS penalty reduces to the adaptive LASSO penalty [39]. Compared with MVMR-PACS, MVMR-PACS-x can achieve improved variable selection performance when the threshold is properly chosen (see the simulation results in Section 2.3). In practice, the threshold can be selected as an additional tuning parameter.

S6 Multifold data thinning for cross validation and postselection inference

S6.1 Multifold data thinning for summary-data MVMR

We adapt the multifold data thinning procedure [25] to summary data MVMR settings to generate multiple independent replicates of summary statistics. Take five-fold data thinning as an example. Let $\epsilon_1, \ldots, \epsilon_5$ be the proportion of information allocated to each generated fold, such that $\sum_{m=1}^{5} \epsilon_m = 1$. For each SNP j, $\hat{\gamma}_j \sim N(\gamma_j, \Sigma_{Xj})$. To generate 5 independent SNP-exposure association estimates, we draw

$$\begin{bmatrix} \hat{\gamma}_{j}^{(1)} \\ \hat{\gamma}_{j}^{(2)} \\ \hat{\gamma}_{j}^{(3)} \\ \hat{\gamma}_{j}^{(3)} \end{bmatrix} \begin{vmatrix} \hat{\epsilon}_{1} \hat{\gamma}_{j} \\ \hat{\epsilon}_{2} \hat{\gamma}_{j} \\ \hat{\gamma}_{j}^{(3)} \\ \hat{\gamma}_{j}^{(4)} \\ \hat{\gamma}_{j}^{(5)} \end{bmatrix} \begin{vmatrix} \hat{\epsilon}_{1} \hat{\gamma}_{j} \\ \hat{\epsilon}_{3} \hat{\gamma}_{j} \\ \hat{\epsilon}_{4} \hat{\gamma}_{j} \\ \hat{\epsilon}_{5} \hat{\gamma}_{j} \end{bmatrix}, \begin{bmatrix} \epsilon_{1} (1 - \epsilon_{1}) \Sigma_{Xj} & -\epsilon_{1} \epsilon_{2} \Sigma_{Xj} & -\epsilon_{1} \epsilon_{3} \Sigma_{Xj} & -\epsilon_{1} \epsilon_{4} \Sigma_{Xj} & -\epsilon_{1} \epsilon_{5} \Sigma_{Xj} \\ -\epsilon_{2} \epsilon_{1} \Sigma_{Xj} & \epsilon_{2} (1 - \epsilon_{2}) \Sigma_{Xj} & -\epsilon_{2} \epsilon_{3} \Sigma_{Xj} & -\epsilon_{2} \epsilon_{4} \Sigma_{Xj} & -\epsilon_{2} \epsilon_{5} \Sigma_{Xj} \\ -\epsilon_{3} \epsilon_{1} \Sigma_{Xj} & -\epsilon_{3} \epsilon_{2} \Sigma_{Xj} & \epsilon_{3} (1 - \epsilon_{3}) \Sigma_{Xj} & -\epsilon_{3} \epsilon_{4} \Sigma_{Xj} & -\epsilon_{3} \epsilon_{5} \Sigma_{Xj} \\ -\epsilon_{4} \epsilon_{1} \Sigma_{Xj} & -\epsilon_{4} \epsilon_{2} \Sigma_{Xj} & -\epsilon_{4} \epsilon_{3} \Sigma_{Xj} & \epsilon_{4} (1 - \epsilon_{4}) \Sigma_{Xj} & -\epsilon_{4} \epsilon_{5} \Sigma_{Xj} \\ -\epsilon_{5} \epsilon_{1} \Sigma_{Xj} & -\epsilon_{5} \epsilon_{2} \Sigma_{Xj} & -\epsilon_{5} \epsilon_{3} \Sigma_{Xj} & -\epsilon_{5} \epsilon_{4} \Sigma_{Xj} & \epsilon_{5} (1 - \epsilon_{5}) \Sigma_{Xj} \end{bmatrix}$$

According to Theorem 2 in [25], we have the following results: (1) for $m = 1, \dots, 5$, $\hat{\gamma}_j^{(m)} \sim N(\epsilon_m \gamma_j, \epsilon_m \Sigma_{Xj})$; (2) $\hat{\gamma}_j^{(1)}, \dots, \hat{\gamma}_j^{(5)}$ are mutually independent; (3) $\hat{\gamma}_j^{(1)} + \hat{\gamma}_j^{(2)} + \dots + \hat{\gamma}_j^{(5)} = \hat{\gamma}_j$. The SNP-outcome association estimates can be generated analogously by replacing $\hat{\gamma}_j$ and Σ_{Xj} with $\hat{\Gamma}_j$ and σ_{Yj}^2 . The generated SNP-outcome association estimate also satisfies: (1) $\hat{\Gamma}_j^{(m)} \sim$

 $N(\epsilon_m \Gamma_j, \epsilon_m \sigma_{Yj}^2)$, where $\Gamma_j = \gamma_j \boldsymbol{\beta}^*$; (2) $\hat{\Gamma}_j^{(1)}, \dots, \hat{\Gamma}_j^{(5)}$ are mutually independent; (3) $\hat{\Gamma}_j^{(1)} + \hat{\Gamma}_j^{(2)} + \dots + \hat{\Gamma}_j^{(5)} = \hat{\Gamma}_j$.

This procedure leads to five independent replicates, D_1, \dots, D_5 of summary statistics for p SNPs: $D_m = \left\{\hat{\gamma}_j^{(m)}, \epsilon_m \Sigma_{Xj}, \hat{\Gamma}_j^{(m)}, \epsilon_m \sigma_{Yj}^2, j = 1, ..., p\right\}$. Importantly, within each replicate, the following relationship holds: $E[\hat{\Gamma}_j^{(m)}] = E[\hat{\gamma}_j^{(m)}] \boldsymbol{\beta}^*$. Therefore, each independent replicate can be in principle used to identify $\boldsymbol{\beta}^*$.

 ϵ_m determines the proportion of instrument strength allocated to the m-th fold. Specifically, the population-level instrument strength matrix [11] based on the D_m is

$$\epsilon_m^{-1} \sum_{j=1}^p \epsilon_m^2 \gamma_j \gamma_j^T \sigma_{Yj}^{-2} = \epsilon_m \sum_{j=1}^p \gamma_j \gamma_j^T \sigma_{Yj}^{-2},$$

which implies that the instrument strength in the m-th fold is ϵ_m of that in the original data. In our implementation, we always let ϵ_m equal each other, corresponding to even information split across generated replicates. We refer interested readers to [25] for discussion on the implication of this parameter. In our implementation, data thinning was performed using the R package datathin which is available at https://github.com/anna-neufeld/datathin.

S6.2 Cross validation based on multifold data thinning

A cross validation procedure can be conducted based on the generated independent replicates through mutlifold data thinning. For example, a 5-fold cross validation can be conducted as follows:

- 1. Create five independent folds of data D_1, \dots, D_5 by applying five-fold data thinning to the original data $D = \left\{ \hat{\gamma}_j, \Sigma_{Xj}, \hat{\Gamma}_j, \sigma_{Yj}^2, j = 1, ..., p \right\}$ of summary statistics with $\epsilon_1, \dots, \epsilon_5$.
- 2. For each fold $m = 1, \ldots, 5$:
 - (a) Define the training set $\mathcal{T}_m = D D_m$ and validation set $\mathcal{V}_m = D_m$. Here, $D D_m = \left\{\hat{\gamma}_j \hat{\gamma}_j^{(m)}, (1 \epsilon_m) \Sigma_{Xj}, \hat{\Gamma}_j \hat{\Gamma}_j^{(m)}, (1 \epsilon_m) \sigma_{Yj}^2, j = 1, ..., p\right\}$, where $\hat{\gamma}_j \hat{\gamma}_j^{(m)} \sim N((1 \epsilon_m) \gamma_j, (1 \epsilon_m) \Sigma_{Xj})$ and $\hat{\Gamma}_j \hat{\Gamma}_j^{(m)} \sim N((1 \epsilon_m) \Gamma_j, (1 \epsilon_m) \sigma_{Yj}^2)$.
 - (b) Fit the model on \mathcal{T}_m (for each candidate tuning parameter λ).
 - (c) Evaluate on \mathcal{V}_m and record the performance metric $L_m(\lambda)$.
- 3. Aggregate performance across folds: $\bar{L}(\lambda) = \frac{1}{5} \sum_{m=1}^{5} L_m(\lambda)$; choose the best tuning parameter $\hat{\lambda}$ according to some criteria, e.g., minimizing $L(\lambda)$.
- 4. Refit the model on the full dataset D using $\hat{\lambda}$.

S6.3 Post-selection inference

To avoid using the same dataset for both model selection and inference, we first perform two-fold data thinning to create two independent datasets, denoted D^{select} and D^{infer} , with even information split. Suppose D^{select} serves as the selection dataset for model and variable selection. We then conduct a five-fold cross validation based on D^{select} according to the algorithm described in Supplementary Section S6.2. This step aims to select tuning parameters and identify signal-groups. In the last step, inference on the identified signal-groups is conducted using SRIVW based on D^{infer} .

S7 Computation and Implementation details

The initial estimates $\tilde{\beta}_{\rm init}$ are obtained by minimizing the projected debiased loss function with a ridge penalty

$$\mathcal{L}_{\text{dRidge}}(\boldsymbol{\beta}, \lambda) = \frac{1}{2} \boldsymbol{\beta}^T (\hat{\Pi}^T W \hat{\Pi} - V)_+ \boldsymbol{\beta} - \hat{\boldsymbol{\Gamma}}^T W \hat{\Pi} \boldsymbol{\beta} + \lambda ||\boldsymbol{\beta}||_2^2.$$
 (S3)

The tuning parameter λ is selected through five-fold data thinning. These initial estimates are also used in defining the adaptive weights in the PACS penalty. We prove the consistency and asymptotic normality of this initial estimator in Section XX of the Supplement. The tuning parameter λ is selected from a grid of values between $[B \times 10^{-4}, B \times 10^2]$ where $B = (\max(\hat{\mu}_{n,min}, 0) + p)^{2/5}$ and $\hat{\mu}_{n,min}$ is the minimum eigenvalue of sample instrument strength matrix [11]. Theorem 1 provides a sufficient condition for the rate of B.

To minimize $\mathcal{L}_{PACS}(\boldsymbol{\beta}, \lambda)$, we adopt the local quadratic approximation approach used in [24]. The main idea is to approximate the non-smooth penalty terms by quadratic functions. For example, by Taylor expansion, for k = 1, ..., K, $|\beta_k| \approx \beta_k^2/(2|\tilde{\beta}_k|) + c$, where $|\tilde{\beta}_k|$ is a given non-zero initial value close to β_k and c is a term irrelevant to β_k . $|\beta_k - \beta_m|$ and $|\beta_k + \beta_m|$ can be approximated in a similar manner. This leads to an efficient iterative algorithm with closed-form updates, as follows:

- 1. Initialize $\boldsymbol{\beta}^{(0)} = \tilde{\boldsymbol{\beta}}_{\text{init}}$.
- 2. At iteration (t+1), calculate

$$\hat{\boldsymbol{\beta}}^{(t+1)} = \left\{ (\hat{\Pi}^T W \hat{\Pi} - V)_+ + \frac{\lambda}{2} (I_w^{(t)} + D_{(-)}^T I_{w(-)}^{(t)} D_{(-)} + D_{(+)}^T I_{w(+)}^{(t)} D_{(+)} \right\}^{-1} \hat{\Pi}^T W \hat{\Gamma}$$

3. Let t = t + 1 and return to Step 2 until convergence.

In the step 2,

$$I_w^{(t)} = \operatorname{diag}(\frac{w_k}{|\hat{\beta}_k^{(t)}|}, j = 1, ..., K)$$

$$I_{w(-)}^{(t)} = \operatorname{diag}(\frac{w_{km(-)}}{|\hat{\beta}_k^{(t)} - \hat{\beta}_m^{(t)}|}, 1 \le k < m \le K)$$

$$I_{w(+)}^{(t)} = \operatorname{diag}\left(\frac{w_{km(+)}}{|\hat{\beta}_k^{(t)} + \hat{\beta}_m^{(t)}|}, 1 \le k < m \le K\right)$$

and $D_{(-)}$ and $D_{(+)}$ are $\frac{K(K-1)}{2} \times K$ matrices of ± 1 that encode all pairwise differences and sums, respectively.

We note that when $(\hat{\Pi}^T W \hat{\Pi} - V)_+$ is positive definite, the objective function $\mathcal{L}_{PACS}(\boldsymbol{\beta}, \lambda)$ is strictly convex and the above algorithm is guaranteed to converge to the global minimizer. When it is only positive semi-definite, e.g., in the presence of highly correlated risk factors, then the algorithm will converge to a local minimizer.

We computed $(\hat{\Pi}^T W \hat{\Pi} - V)_+$ using the ADMM_proj function from the R package BDcocolasso which is available at https://github.com/celiaescribe/BDcocolasso.

S8 Proofs

We denote the sample sizes for the outcome and each exposure as $n_Y, n_{Xk}, k = 1, ..., K$, respectively. Let diag $(a_1, ..., a_K)$ denote a $K \times K$ diagonal matrix with diagonal entries $a_1, ..., a_K$. We make the following assumption on the observed data.

Assumption 1. (i) The sample sizes $n_Y, n_{Xk}, k = 1, ..., K$ diverge to infinity at the same rate. Let $n = \min(n_Y, n_{X1}, ..., n_{XK})$. The number of exposures K and the number of SNPs p grow to infinity as n increases.

(ii) The 2p random vectors (variables) $\{\hat{\gamma}_j, \hat{\Gamma}_j, j = 1, ..., p\}$ are mutually independent. For each $j, \hat{\gamma}_j \sim N(\gamma_j, \Sigma_{Xj}), \hat{\Gamma}_j \sim N(\Gamma_j, \sigma_{Yj}^2), \Gamma_j = \gamma_j^T \boldsymbol{\beta}^*$.

(iii) The variances $\Sigma_{Xj} = \operatorname{diag}(\sigma_{Xj1}, \ldots, \sigma_{XjK}) \Sigma \operatorname{diag}(\sigma_{Xj1}, \ldots, \sigma_{XjK})$ and σ_{Yj}^2 are known, where σ_{Xjk} is the SE of $\hat{\gamma}_{jk}$ and Σ represents a positive definite shared correlation matrix. Moreover, the variance ratios $\sigma_{Xjk}^2/\sigma_{Yj}^2$ are bounded away from zero and infinity for all $j=1,\ldots,p$ and $k=1,\ldots,K$.

Assumption 2. There exists a non-random $K \times K$ matrix $S_n = \tilde{S}_n \operatorname{diag}(\sqrt{\mu_{n1}}, ..., \sqrt{\mu_{nK}})$ that satisfy the following conditions: (i) \tilde{S}_n is bounded element-wise and the smallest eigenvalue of $\tilde{S}_n \tilde{S}_n^T$ is bounded away from 0, and (ii) $S_n^{-1} \left(\sum_{j=1}^p \gamma_j \gamma_j^T \sigma_{Y_j}^{-2} \right) S_n^{-T}$ is bounded element-wise and its smallest eigenvalue is bounded away from 0.

These two assumptions are also made in [11] with detailed discussions. In particular, Assumption 2 provides a general asymptotic regime to study MVMR estimators, allowing for varying degrees of instrument strengths across different combinations of exposures. The vector $\mu_{n1}, \ldots, \mu_{nK}$ represents a complete, multi-dimensional summary of overall instrument strength, and the scalar $\mu_{n,\min} = \min(\mu_{n1}, \ldots, \mu_{nK})$ captures the slowest rate among all linear combinations of exposures. We further assume all the standard error estimates as well as the shared correlation matrix Σ can be estimated with negligible errors and hence are considered as known quantities. Additionally, note that $\gamma_j, \Gamma_j, \Sigma_{Xj}, \sigma_{Yj}, j = 1, \ldots, p$ are sequences of real numbers or matrices that can depend on n in theoretical analysis, but we omit the n index for ease of notation.

S8.1 MVMR-dRidge

The oracle properties of MVMR-PACS (see Theorem 1) require a consistent and asymptotic normal initial estimator. Theorem 1 establishes the consistency and asymptotic normality of MVMR-dRidge (MVMR debiased ridge estimator), which is used as the initial estimator. MVMR-dRidge is the unique minimizer to the following loss function:

$$\hat{\boldsymbol{\beta}}_{\text{dRidge}} = \arg\min_{\boldsymbol{\beta}} \frac{1}{2} \boldsymbol{\beta}^T (\hat{\Pi}^T W \hat{\Pi} - V)_{+} \boldsymbol{\beta} - \hat{\boldsymbol{\Gamma}}^T W \hat{\Pi} \boldsymbol{\beta} + \phi ||\boldsymbol{\beta}||_2^2.$$
 (S4)

 $\hat{\beta}_{\text{dRidge}}$ has a closed-form solution:

$$\hat{\boldsymbol{\beta}}_{\text{dRidge}} = ((\hat{\Pi}^T W \hat{\Pi} - V)_+ + \phi I_K)^{-1} \hat{\Pi} W \hat{\Gamma}.$$

Theorem 1. Assume Assumptions 1-2, $\mu_{n,\min}/\sqrt{p} \to \infty$, and $\max_j \gamma_{jk}^2 \sigma_{Xjk}^{-2}/(\mu_{n,\min} + p) \to 0$ for all k as $n \to \infty$. If $\phi = o_P(\sqrt{\mu_{n,\min} + p})$, where $a_n = O_P(b_n)$ means a_n/b_n is bounded in probability, then $\hat{\beta}_{dRidge}$ is consistent and asymptotically normal, i.e., as $n \to \infty$,

$$\mathbb{V}^{-\frac{1}{2}} \left\{ \sum_{j=1}^{p} M_j \right\} (\hat{\boldsymbol{\beta}}_{\text{dRidge}} - \boldsymbol{\beta}_0) \xrightarrow{d} N(\mathbf{0}, I_K), \tag{S5}$$

where
$$M_j = \gamma_j \gamma_j^T \sigma_{Y_j}^{-2}$$
, $V_j = \Sigma_{X_j} \sigma_{Y_j}^{-2}$, and $\mathbb{V} = \sum_{j=1}^p \{ (1 + \beta_0^T V_j \beta_0) (M_j + V_j) + V_j \beta_0 \beta_0^T V_j \}$.

The proof largely mirrors the proof for Theorem 2 in [11], and hence is omitted. The key modification is to show $\phi \mathbb{V}^{-\frac{1}{2}}(\sum_j M_j)^{-1}\mathbb{V}^{\frac{1}{2}} = o_p(1)$ and $\phi \mathbb{V}^{-\frac{1}{2}} = o_p(1)$. In practice, we constructed a logarithmically spaced grid of candidate penalty values for ϕ , ranging from 10^2 to 10^{-4} times an upper bound that scales with $\hat{\mu}_{n,\min} + p$ when $\hat{\mu}_{n,\min} \geq 0$, and scales with p when $\hat{\mu}_{n,\min} < 0$.

S8.2 MVMR-dLASSO

MVMR-dLASSO is the unique minimizer to the following loss function:

$$\hat{\boldsymbol{\beta}}_{\text{dLASSO}} = \underset{\boldsymbol{\beta}}{\operatorname{arg\,min}} \frac{1}{2} \boldsymbol{\beta}^T (\hat{\Pi}^T W \hat{\Pi} - V)_{+} \boldsymbol{\beta} - \hat{\boldsymbol{\Gamma}}^T W \hat{\Pi} \boldsymbol{\beta} + \lambda_n \sum_{k} \hat{w}_k |\beta_k|.$$

where $\hat{w}_k = 1/|\tilde{\beta}_k|^{\tau}$ and $\tilde{\boldsymbol{\beta}}_{\text{init}} = (\tilde{\beta}_1, \dots, \tilde{\beta}_K)^T$ is a consistent and asymptotically normal estimator of $\boldsymbol{\beta}^*$ under the assumptions of Theorem 1.

MVMR-dLASSO is the unique minimizer to the following objective function:

$$\hat{\boldsymbol{\beta}}_{\text{dLASSO}}^{(n)} = \underset{\boldsymbol{\beta}}{\operatorname{arg\,min}} \frac{1}{2} \boldsymbol{\beta}^T (\hat{\Pi}^T W \hat{\Pi} - V)_{+} \boldsymbol{\beta} - \hat{\boldsymbol{\Gamma}}^T W \hat{\Pi} \boldsymbol{\beta} + \lambda_n \sum_{k} \hat{w}_k |\beta_k|$$

where $\hat{w}_k = 1/|\tilde{\beta}_k|^{\tau}$ and $\tilde{\boldsymbol{\beta}}_{\text{init}} = (\tilde{\beta}_1, \dots, \tilde{\beta}_K)^T$ is a consistent and asymptotically normal estimator of $\boldsymbol{\beta}^*$ under the assumptions of Theorem 1.

Theorem 2. (Oracle properties of MVMR-dLASSO) Under Assumptions 3-2, $\mu_{n,\min}/\sqrt{p} \to \infty$, and $\max_j \gamma_{jk}^2 \sigma_{Xjk}^{-2}/(\mu_{n,\min}+p) \to 0$ for all k as $n \to \infty$, suppose that $\lambda_n/r_n \to 0$, $\lambda_n r_n^{\tau-1} \to \infty$ where $r_n = \mu_{n,\min}/\sqrt{\mu_{n,\min}+p}$ and τ satisfies $\lambda_n r_n^{\tau+1}/\mu_{n,\max} \to \infty$, then

- 1. Consistency in risk factor selection: $\lim_n \mathbb{P}(A_n = A) = 1$
- 2. Asymptotic normality: $\mathbb{V}_{\mathcal{A}}^{-\frac{1}{2}}(\Pi^T W \Pi)_{\mathcal{A}}(\hat{\beta}_{\text{dLASSO},\mathcal{A}}^{(n)} \boldsymbol{\beta}_{\mathcal{A}}^*) \xrightarrow{D} N(\mathbf{0}, I_{|\mathcal{A}|})$

where $\mathcal{A} = \{k : \beta_k^* \neq 0\}$, $\mathcal{A}_n = \{k : \hat{\beta}_{\text{dLASSO},k}^{(n)} \neq 0\}$, and $\mathbb{V} = \sum_{j=1}^p \{(1 + \boldsymbol{\beta}^{*T} V_j \boldsymbol{\beta}^*)(M_j + V_j) + V_j \boldsymbol{\beta} \boldsymbol{\beta}^{*T} V_j\}$, $I_{|\mathcal{A}|}$ is an identity matrix of size $|\mathcal{A}| \times |\mathcal{A}|$, and the subscript \mathcal{A} applied to a vector (or matrix) denotes the subvector (or submatrix) formed by selecting the entries (or rows and columns) corresponding to the indices in the set \mathcal{A} .

Proof. The proof follows the proof of adaptive LASSO in [39] with adaption of a random design matrix and non-i.i.d. setup. To ease the notation, we remove the subscript dLASSO in the objective function and MVMR-dLASSO estimator in this proof. Under Assumption 2 and by Lemma 7 in [11] that $S_n^{-1}(\hat{\Pi}^T W \hat{\Pi} - \Pi^T W \Pi - V) S_n^{-T} \xrightarrow{P} \mathbf{0}$, we know the minimum eigenvalue of $\hat{\Pi}^T W \hat{\Pi} - V$ is $\Theta_p(\mu_{n,\min})$. Because we have assumed that $\mu_{n,\min}/\sqrt{p} \to \infty$, $(\hat{\Pi}^T W \hat{\Pi} - V)_+ = \hat{\Pi}^T W \hat{\Pi} - V$ for large n. Therefore, for large n, the objective function for MVMR-dLASSO can be simplified as

$$\Psi^{(n)}(\boldsymbol{\beta}) = \frac{1}{2}\boldsymbol{\beta}^T (\hat{\Pi}^T W \hat{\Pi} - V) \boldsymbol{\beta} - \hat{\boldsymbol{\Gamma}}^T W \hat{\Pi} \boldsymbol{\beta} + \lambda_n \sum_k \hat{w}_k |\beta_k|$$

Define $\mathbf{u} = r_n(\boldsymbol{\beta} - \boldsymbol{\beta}^*)$. Then, $\boldsymbol{\beta} = \boldsymbol{\beta}^* + \frac{\mathbf{u}}{r_n}$, where under the assumption $\mu_{n,\min}/\sqrt{p} \to \infty$, $r_n \to \infty$. Then, the objective function can be writen as a function of \mathbf{u} as follows

$$\Psi^{(n)}(\boldsymbol{u}) = \frac{1}{2}(\boldsymbol{\beta}^* + \frac{\boldsymbol{u}}{r_n})^T (\hat{\Pi}^T W \hat{\Pi} - V)(\boldsymbol{\beta}^* + \frac{\boldsymbol{u}}{r_n}) - \hat{\Gamma}^T W \hat{\Pi}(\boldsymbol{\beta}^* + \frac{\boldsymbol{u}}{r_n}) + \lambda_n \sum_{k=1} \hat{w}_k |\beta_k^* + \frac{u_k}{r_n}|$$

Let $\hat{\boldsymbol{u}}^{(n)} = \arg\min \Psi^{(n)}(\boldsymbol{u})$. The goal is then to figure out the asymptotic properties of $\hat{\boldsymbol{u}}^{(n)}$. Once we know the properties of $\hat{\boldsymbol{u}}^{(n)}$, we know the properties of $\hat{\boldsymbol{\beta}}^{(n)}$ because $\hat{\boldsymbol{\beta}}^{(n)} = \boldsymbol{\beta}^* + \frac{\hat{\boldsymbol{u}}^{(n)}}{r_n}$.

Define $V^{(n)}(\boldsymbol{u}) = \Psi_n(\boldsymbol{u}) - \Psi_n(\boldsymbol{0})$. Specifically,

$$V^{(n)}(\boldsymbol{u}) = \frac{1}{2r_n^2} \boldsymbol{u}^T (\hat{\Pi}^T W \hat{\Pi} - V) \boldsymbol{u} - \frac{1}{r_n} \boldsymbol{u}^T (\hat{\Pi}^T W \hat{\Gamma} - \hat{\Pi}^T W \hat{\Pi} \boldsymbol{\beta}^* + V \boldsymbol{\beta}^*)$$
$$+ \lambda_n \sum_{k=1} \hat{w}_k \{ |\beta_k^* + \frac{u_k}{r_n}| - |\beta_k^*| \}$$

For the first term, by assumption 2 and Lemma 7 in [11] that $S_n^{-1}(\hat{\Pi}^T W \hat{\Pi} - \Pi^T W \Pi - V) S_n^{-T} \xrightarrow{P}$ **0**, the minimum and maximum eigenvalue of $\hat{\Pi}^T W \hat{\Pi} - V$ are of order $\Theta(\mu_{n,\text{min}})$ and $\Theta(\mu_{n,max})$, respectively. Then, for every \boldsymbol{u} , we have

$$\frac{1}{r_n^2} \boldsymbol{u}^T (\hat{\Pi}^T W \hat{\Pi} - V) \boldsymbol{u} = O_p(\frac{\mu_{n,\text{max}}}{r_n^2}), \tag{S6}$$

and $\frac{1}{r_n^2}(\hat{\Pi}^TW\hat{\Pi}-V)$ remains positive definite with high probability as $n\to\infty$ because the minimum eigenvalue of $\frac{1}{r_n^2}(\hat{\Pi}^TW\hat{\Pi}-V)=\Theta_p(\frac{\mu_{n,\min}+p}{\mu_{n,\min}})\geq\Theta_p(1)$. This ensures that $V^{(n)}(\boldsymbol{u})$ is a strictly convex function of \boldsymbol{u} for large n, and $\hat{\boldsymbol{u}}^{(n)}$ is unique and bounded.

For the third term, we consider its behavior as $n \to \infty$. For $\beta_k^* \neq 0$, we have $\hat{w}_k \stackrel{P}{\to} |\beta_k^*|^{-\tau}$ by the assumption that $\tilde{\beta}_{\text{init}}$ is consistent, and $r_n(|\beta_k^* + \frac{u_k}{r_n}| - |\beta_k^*|) \to u_k \text{sign}(\beta_k^*)$. Hence, $\lambda_n \hat{w}_k(|\beta_k^* + \frac{u_k}{r_n}| - |\beta_k^*|)$

 $|\beta_k^*|) = O_p(\frac{\lambda_n}{r_n})u_k \mathrm{sign}(\beta_k^*), \forall k \in \mathcal{A}. \text{ Under the assumption that } \lambda_n/r_n \to 0, \text{ we have } \lambda_n \hat{w}_k \{|\beta_k^* + \frac{u_k}{r_n}| - |\beta_k^*|\} = \frac{\lambda_n}{r_n} \hat{w}_k \left[r_n \{|\beta_k^* + \frac{u_k}{r_n}| - |\beta_k^*|\} \right] = o_p(1). \text{ For } \beta_k^* = 0, r_n \{|\beta_k^* + \frac{u_k}{r_n}| - |\beta_k^*|\} = |u_k|. \text{ Because } \\ \tilde{\boldsymbol{\beta}}_{\text{init}} \text{ is also asymptotically normal, } [\mathcal{V}_n]_{kk}^{-1} \tilde{\beta}_k \xrightarrow{D} N(0,1) = O_p(1), \text{ where } \mathcal{V}_n \text{ is a consistent estimator of the asymptotic variance of } \tilde{\boldsymbol{\beta}}_{\text{init}}. \text{ Thus, } \lambda_n \hat{w}_k |\frac{u_k}{r_n}| = \frac{\lambda_n}{r_n} [\mathcal{V}_n]_{kk}^{-\frac{\tau}{2}} |u_k| \{[\mathcal{V}_n]_{kk}^{-\frac{1}{2}} \tilde{\beta}_k\}^{-\tau}. \text{ The slowest rate at which the diagonal term of } \mathcal{V}_n \text{ goes to 0 is } r_n^{-2} \text{ by Lemma 8 in [11]. By the assumption that } \lambda_n r_n^{\tau-1} \to \infty, \text{ we have } \lambda_n \hat{w}_k \{|\beta_k^* + \frac{u_k}{r_n}| - |\beta_k^*|\} \to \infty \text{ with probability tending one. This holds true unless } \hat{u}_k^{(n)} \text{ goes to 0 sufficiently fast, faster than } \lambda_n r_n^{\tau-1}.$

We now show that $\hat{\boldsymbol{u}}_{\mathcal{A}^c}^{(n)} \stackrel{P}{\to} \boldsymbol{0}$. Suppose for contradiction that there exists $\epsilon > 0$ and an index $k \in \mathcal{A}^c$, such that, the event $|\hat{u}_k^{(n)}| \geq \epsilon$ happens infinitely often. This implies that $\lambda_n \hat{w}_k \{|\beta_k^* + \frac{\hat{u}_k^{(n)}}{r_n}| - |\beta_k^*|\} \geq \frac{\lambda_n}{r_n} \hat{w}_k \epsilon$ with probability tending one. As discussed above, when $\beta_k^* = 0$, $\frac{\lambda_n}{r_n} \hat{w}_k = O_p(\lambda_n r_n^{\tau-1}) \to \infty$. Furthermore, by the result (S6) and boundedness of $\hat{\boldsymbol{u}}^{(n)}$, the rate $\frac{1}{r_n^2} \hat{\boldsymbol{u}}^{(n)T} (\hat{\Pi}^T W \hat{\Pi} - V) \hat{\boldsymbol{u}}^{(n)}$ diverges to infinity is at most $\mu_{n,\max}/r_n^2$. By the assumption that $\lambda_n r_n^{\tau+1}/\mu_{n,\max} \to \infty$, we have $\lambda_n \hat{w}_k \{|\beta_k^* + \frac{u_k^{(n)}}{r_n}| - |\beta_k^*|\}$ goes to infinity at a rate faster than $\frac{1}{r_n^2} \hat{\boldsymbol{u}}^{(n)T} (\hat{\Pi}^T W \hat{\Pi} - V) \hat{\boldsymbol{u}}^{(n)}$ for any $\hat{\boldsymbol{u}}^{(n)}$ that has $|\hat{u}_k^{(n)}| \geq \epsilon$ happens infinitely often. Consequently, the objective function $\Psi_n(\hat{\boldsymbol{u}}^{(n)})$ goes to infinity with probability tending one. However, this contradicts the definition of $\hat{\boldsymbol{u}}^{(n)}$ as the minimizer of $\Psi^{(n)}$ because we could always pick $\hat{\boldsymbol{u}}^{(n)}$ with $\hat{u}_k^{(n)} = 0$, $\forall k \in \mathcal{A}^c$ and other coordinates suitably to make the objective function smaller. Hence, we must have $\hat{u}_k^{(n)} \stackrel{P}{\to} 0$, $\forall k \in \mathcal{A}^c$.

As a result, for large enough n, we only need to minimize

$$\frac{1}{2r_n^2}\boldsymbol{u}_{\mathcal{A}}^T(\hat{\Pi}^TW\hat{\Pi}-V)_{\mathcal{A}}\boldsymbol{u}_{\mathcal{A}}-\frac{1}{r_n}\boldsymbol{u}_{\mathcal{A}}^T(\hat{\Pi}^TW\hat{\Gamma}-\hat{\Pi}^TW\hat{\Pi}\boldsymbol{\beta}^*+V\boldsymbol{\beta}^*)_{\mathcal{A}}+O_p(\frac{\lambda_n}{r_n})\boldsymbol{u}_{\mathcal{A}}^T\cdot\operatorname{sign}(\boldsymbol{\beta}_{\mathcal{A}}^*).$$

This objective is convex and the minimizer is

$$\hat{\boldsymbol{u}}_{\mathcal{A}}^{(n)} = r_n(\hat{\Pi}^T W \hat{\Pi} - V)_{\mathcal{A}}^{-1}(\hat{\Pi}^T W \hat{\boldsymbol{\Gamma}} - \hat{\Pi}^T W \hat{\Pi} \boldsymbol{\beta}^* + V \boldsymbol{\beta}^*)_{\mathcal{A}} + O_p(\lambda_n r_n)(\hat{\Pi}^T W \hat{\Pi} - V)_{\mathcal{A}}^{-1} \mathrm{sign}(\boldsymbol{\beta}_{\mathcal{A}}^*)$$

This implies that,

$$(\hat{\boldsymbol{\beta}}_{\mathcal{A}}^{(n)} - \boldsymbol{\beta}_{\mathcal{A}}^{*}) = (\hat{\Pi}^{T} W \hat{\Pi} - V)_{\mathcal{A}}^{-1} (\hat{\Pi}^{T} W \hat{\Gamma} - \hat{\Pi}^{T} W \hat{\Pi} \boldsymbol{\beta}^{*} + V \boldsymbol{\beta}^{*})_{\mathcal{A}} + O_{p}(\lambda_{n}) (\hat{\Pi}^{T} W \hat{\Pi} - V)_{\mathcal{A}}^{-1} \operatorname{sign}(\boldsymbol{\beta}_{\mathcal{A}}^{*}),$$
 and then,

$$\mathbb{V}_{\mathcal{A}}^{-\frac{1}{2}}(\Pi^{T}W\Pi)_{\mathcal{A}}(\hat{\boldsymbol{\beta}}_{\mathcal{A}}^{(n)} - \boldsymbol{\beta}_{\mathcal{A}}^{*}) = \mathbb{V}_{\mathcal{A}}^{-\frac{1}{2}}(\Pi^{T}W\Pi)_{\mathcal{A}}(\hat{\Pi}^{T}W\hat{\Pi} - V)_{\mathcal{A}}^{-1}(\hat{\Pi}^{T}W\hat{\Gamma} - \hat{\Pi}^{T}W\hat{\Pi}\boldsymbol{\beta}^{*} + V\boldsymbol{\beta}^{*})_{\mathcal{A}}
+ O_{p}(\lambda_{n}r_{n})(\hat{\Pi}^{T}W\hat{\Pi} - V)_{\mathcal{A}}^{-1}\operatorname{sign}(\boldsymbol{\beta}_{\mathcal{A}}^{*})
= \underbrace{\mathbb{V}_{\mathcal{A}}^{-\frac{1}{2}}(\Pi^{T}W\Pi)_{\mathcal{A}}(\hat{\Pi}^{T}W\hat{\Pi} - V)_{\mathcal{A}}^{-1}\mathbb{V}_{\mathcal{A}}^{\frac{1}{2}}\underbrace{\mathbb{V}_{\mathcal{A}}^{-\frac{1}{2}}(\hat{\Pi}^{T}W\hat{\Gamma} - \hat{\Pi}^{T}W\hat{\Pi}\boldsymbol{\beta}^{*} + V\boldsymbol{\beta}^{*})_{\mathcal{A}}}_{A_{2}}
+ O_{p}(\lambda_{n})\underbrace{\mathbb{V}_{\mathcal{A}}^{-\frac{1}{2}}(\Pi^{T}W\Pi)_{\mathcal{A}}(\hat{\Pi}^{T}W\hat{\Pi} - V)_{\mathcal{A}}^{-1}\mathbb{V}_{\mathcal{A}}^{\frac{1}{2}}\mathbb{V}_{\mathcal{A}}^{-\frac{1}{2}}\operatorname{sign}(\boldsymbol{\beta}_{\mathcal{A}}^{*})}$$

By the result S10 and Lemma 6 in [11], we know $A_1 \xrightarrow{P} I_{|\mathcal{A}|}$ and $A_2 \xrightarrow{D} N(\mathbf{0}, I_{|\mathcal{A}|})$. Additionally,

by Lemma 2 in [11], $\mathbb{V}_{\mathcal{A}}^{-\frac{1}{2}}$ goes to 0 at a rate at least $\sqrt{\mu_{n,\min}+p}$. Thus, the second term is of order $O_p(\lambda_n/\sqrt{\mu_{n,\min}+p}) = o_p(1)$ as $\lambda_n/r_n \to 0$. Lastly, by the Slutsky's theorem, we complete the proof of the asymptotic normality part. That is,

$$\mathbb{V}_{\mathcal{A}}^{-\frac{1}{2}}(\Pi^T W \Pi)_{\mathcal{A}}(\hat{\boldsymbol{\beta}}_{\mathcal{A}}^{(n)} - \boldsymbol{\beta}_{\mathcal{A}}^*) \xrightarrow{D} N(0, I_{|\mathcal{A}|}) = O_p(1). \tag{S7}$$

To show the selection consistency part, note that $\forall k \in \mathcal{A}$, by the asymptotic normality result, we have $\hat{\beta}_k^{(n)} \xrightarrow{P} \beta_k^*$. Thus, $\mathbb{P}(k \in \mathcal{A}_n) \to 1$. It remains to show that $\forall k' \in \mathcal{A}^c$, $\mathbb{P}(k' \in \mathcal{A}_n) \to 0$. Consider the event $k' \in \mathcal{A}_n$ (i.e. $\hat{\beta}_{k'}^{(n)} \neq 0$), by the KKT conditions, we know $\hat{\beta}^{(n)}$ satisfies

$$\left[(\hat{\Pi}^T W \hat{\Pi} - V) \hat{\boldsymbol{\beta}}^{(n)} - \hat{\Pi}^T W \hat{\boldsymbol{\Gamma}} \right]_{k'} = \lambda_n \hat{w}_{k'} \operatorname{sign}(\hat{\beta}_{k'}^{(n)})$$
 (S8)

where $[\boldsymbol{v}]_k$ means the k-th entry of the vector \boldsymbol{v} . The right hand side $\lambda_n \hat{w}_{k'} \to \infty$ at a rate $\lambda_n r_n^{\tau}$ as we have shown above. For the left hand side, note that

$$(\hat{\Pi}^T W \hat{\Pi} - V) \hat{\boldsymbol{\beta}}^{(n)} - \hat{\Pi}^T W \hat{\boldsymbol{\Gamma}} = (\hat{\Pi}^T W \hat{\Pi} - V) (\hat{\boldsymbol{\beta}}^{(n)} - \boldsymbol{\beta}^*) - \mathbb{V}^{\frac{1}{2}} \left\{ \mathbb{V}^{-\frac{1}{2}} (\hat{\Pi}^T W \hat{\boldsymbol{\Gamma}} - \hat{\Pi}^T W \hat{\Pi} \boldsymbol{\beta}^* + V \boldsymbol{\beta}^*) \right\}$$

From Lemma 6 in [11], we know $\mathbb{V}^{-\frac{1}{2}}(\hat{\Pi}^T W \hat{\Gamma} - \hat{\Pi}^T W \hat{\Pi} \boldsymbol{\beta}^* + V \boldsymbol{\beta}^*) = O_p(1)$ and hence the fast rate at which $\mathbb{V}^{\frac{1}{2}} \left\{ \mathbb{V}^{-\frac{1}{2}}(\hat{\Pi}^T W \hat{\Gamma} - \hat{\Pi}^T W \hat{\Pi} \boldsymbol{\beta}^* + V \boldsymbol{\beta}^*) \right\}$ diverges is $\sqrt{\mu_{n,\max} + p}$. For the first term,

we study its k' entry. Let v_k denote the k-th row of $\hat{\Pi}^T W \hat{\Pi} - V$. We know $v_k = O_p(\mu_{n,\text{max}})$ by Assumption 2 and Lemma 7 in [11]. Then, the k' entry of the first term equals

$$v_{k',\mathcal{A}}(\hat{\boldsymbol{\beta}}^{(n)} - \boldsymbol{\beta}^*)_{\mathcal{A}} + v_{k',\mathcal{A}^c}(\hat{\boldsymbol{\beta}}^{(n)} - \boldsymbol{\beta}^*)_{\mathcal{A}^c} = v_{k',\mathcal{A}}(\Pi^T W \Pi)_{\mathcal{A}}^{-1} \mathbb{V}_{\mathcal{A}}^{\frac{1}{2}} \mathbb{V}_{\mathcal{A}}^{-\frac{1}{2}}(\Pi^T W \Pi)_{\mathcal{A}}(\hat{\boldsymbol{\beta}}^{(n)} - \boldsymbol{\beta}^*)_{\mathcal{A}} + v_{k',\mathcal{A}^c}\hat{\boldsymbol{\beta}}_{\mathcal{A}^c}^{(n)}.$$

We have shown in (S7) that $\mathbb{V}_{\mathcal{A}}^{-\frac{1}{2}}(\Pi^T W \Pi)_{\mathcal{A}}(\hat{\boldsymbol{\beta}}^{(n)} - \boldsymbol{\beta}^*)_{\mathcal{A}} = O_p(1)$. Additionally, $(\Pi^T W \Pi)_{\mathcal{A}}^{-1} \mathbb{V}_{\mathcal{A}}^{\frac{1}{2}}$ goes to 0 at a rate of at least r_n by Lemma 8 in [11]. Thus, the first term is $O_p(\mu_{n,\max}/r_n)$. The second term is also $O_p(\mu_{n,\max}/r_n)$ as we have shown that $\hat{\boldsymbol{u}}_{\mathcal{A}^c} \xrightarrow{P} \mathbf{0}$ and $\hat{\boldsymbol{\beta}}_{\mathcal{A}^c}^{(n)} = \hat{\boldsymbol{u}}_{\mathcal{A}^c}/r_n$. In

summary,
$$\left[(\hat{\Pi}^T W \hat{\Pi} - V) \hat{\boldsymbol{\beta}}^{(n)} - \hat{\Pi}^T W \hat{\boldsymbol{\Gamma}} \right]_{k'} \text{ is } O_p(\max\{\mu_{n,\max}/r_n, \sqrt{\mu_{n,\max} + p}\}) = O_p(\mu_{n,\max}/r_n),$$

because it is easy to see that $\mu_{n,\max}/\sqrt{\mu_{n,\max}+p} \geq \mu_{n,\min}/\sqrt{\mu_{n,\min}+p} = r_n$. Finally, because $\lambda_n r_n^{\tau+1}/\mu_{n,\max} \to \infty$, we conclude that the equation (S8) cannot hold because the right hand side grows faster than the left hand side as $n \to \infty$. This is a contradiction and therefore we must have $\forall k' \in \mathcal{A}^c$, $\mathbb{P}(k' \in \mathcal{A}_n) \to 0$.

S8.3 MVMR-PACS

MVMR-PACS is the unique minimizer to the following objective function:

$$\hat{\boldsymbol{\beta}}_{PACS}^{(n)} = \arg\min_{\boldsymbol{\beta}} \frac{1}{2} \boldsymbol{\beta}^T (\hat{\Pi}^T W \hat{\Pi} - V)_{+} \boldsymbol{\beta} - \hat{\boldsymbol{\Gamma}}^T W \hat{\Pi} \boldsymbol{\beta} + \lambda_n P(\boldsymbol{\beta})$$

where $P(\boldsymbol{\beta}) = \sum_{k=1}^{K} \hat{w}_k |\beta_k| + \sum_{k < m} \hat{w}_{km(-)} |\beta_k - \beta_m| + \sum_{k < m} \hat{w}_{km(+)} |\beta_k + \beta_m|, \ \hat{w}_k = 1/|\tilde{\beta}_k|^{\tau}, \ \hat{w}_{km(-)} = \hat{c}_{km(-)}/|\tilde{\beta}_k - \tilde{\beta}_m|^{\tau}, \ \hat{w}_{km(+)} = \hat{c}_{km(+)}/|\tilde{\beta}_k + \tilde{\beta}_m|^{\tau}, \ \text{and} \ \tilde{\beta}_{\text{init}} = (\tilde{\beta}_1, \dots, \tilde{\beta}_K)^T \text{ is a consistent and asymptotically normal estimator of } \boldsymbol{\beta}^* \text{ under the assumption of Theorem 1, } c_{km(-)}^{(n)} \ \text{and} \ c_{km(+)}^{(n)} \ \text{are user-specified and potentially data-dependent weights. In our setting, } c_{km(-)}^{(n)} \ \text{and} \ c_{km(+)}^{(n)} \ \text{are given in the main text section } 4.4. \ \text{We require } \hat{c}_{km(-)} \xrightarrow{P} c_{km(-)}, \ \text{and} \ \hat{c}_{km(+)} \xrightarrow{P} c_{km(+)} \ \text{that satisfy } 0 < c_{km(-)}, c_{km(+)} < \infty \ \text{for all } k, m \in \{1, \dots, K\}.$

Let $\bar{\gamma}_j = G\gamma_j$ be the true association of j-th SNP with L causal groups, where G follows the definition given in the main text section 4.8. In words, G collapses elements of γ_j by taking the sum (difference) if the corresponding true causal effects are nonzero and of the same (opposite) magnitude and it drops elements of γ_j if the corresponding true causal effects are zero.

Lemma S1. For the matrices G and C_g satisfying the definition given in the main text section 4.8, $G^TC_g\beta^* = \beta^*$.

Proof. Recall that for each risk factor k, if it belongs to a causal group G_l (i.e. $k \in G_l$ for some l), then $\beta_k^* = s_k \alpha_l$, where $s_k \in \{-1, +1\}$ and $\alpha_l > 0$ represents the magnitude of the causal effect of group G_l ; otherwise, $\beta_k^* = 0$, i.e., it is a non-causal risk factor.

Next, note that for every $k, j \in \{1, ..., K\}$,

$$(G^T C_g)_{(k,j)} = \sum_{l=1}^{L} G_{kl} C_{g,jl} = \begin{cases} \frac{s_k s_j}{|G_l|}, & \text{if } \exists l(k) \in \{1, ..., L\} \text{ s.t. } k, j \in G_{l(k)} \\ 0, & \text{otherwise} \end{cases}$$

where l(k) denotes the unique group index such that $k \in G_{l(k)}$. In other words, $(G^T C_g)_{(k,j)}$ is only non-zero when k, l belong to the same causal group, and zero otherwise.

Now we consider $G^TC_q\beta^*$. Its k-th component is

$$(G^T C_g \boldsymbol{\beta}^*)_k = \sum_{j=1}^K (G^T C_g)_{kj} \beta_j^*$$

There are two scenarios. First, if risk factor k is non-causal, then $(G^TC_g)_{kj} = 0$ for all j = 1, ..., K. Then, $(G^TC_g\beta^*)_k = \beta_k^* = 0$. Second, if risk factor k is causal, then there exists l(k) such that $k \in G_{l(k)}$ and

$$\begin{split} (G^T C_g \beta^*)_k &= \sum_{j=1}^K (G^T C_g)_{kj} \beta_j^* \\ &= \sum_{j \in G_{l(k)}} (G^T C_g)_{kj} \beta_j^* \text{ as } (G^T C_g)_{kj} \text{ is non-zero only if } k, j \text{ belong to the same causal group} \\ &= \sum_{j \in G_{l(k)}} \frac{s_k s_j}{|G_{l(k)}|} \beta_j^* \\ &= \sum_{j \in G_{l(k)}} \frac{s_k s_j}{|G_{l(k)}|} s_j \alpha_{l(k)} \text{ as } \beta_j^* = s_j \alpha_{l(k)} \end{split}$$

$$= \sum_{j \in G_{l(k)}} \frac{s_k}{|G_{l(k)}|} \alpha_{l(k)}$$
$$= s_k \alpha_{l(k)} \sum_{j \in G_{l(k)}} \frac{1}{|G_{l(k)}|}$$
$$= s_k \alpha_{l(k)} = \beta_k^*$$

This completes the proof.

Theorem 3. (Oracle properties of MVMR-PACS) Under the same conditions as in Theorem 2, the MVMR-PACS estimator satisfies

- 1. Consistency in risk factor selection: $\lim_n \mathbb{P}(\mathcal{B}_n = \mathcal{B}) = 1$
- 2. Asymptotic normality: $\mathbb{V}_g^{-\frac{1}{2}}(\Pi_g^T W \Pi_g)(C_g \hat{\beta}_{PACS}^{(n)} C_g \beta^*) \xrightarrow{D} N(\mathbf{0}, I_L)$

where $\mathcal{B} = \{k : \theta_k \neq 0\}$, $\mathcal{B}_n = \{k : \hat{\beta}_{PACS,k}^{(n)} \neq 0\}$, and $\Pi_g = \Pi G^T$, $V_{j,g} = G \Sigma_{Xj} \sigma_{Yj}^{-2} G^T$, $\mathbb{V}_g = \sum_{j=1}^p \{(1 + \bar{\boldsymbol{\beta}}^{*T} V_{j,g} \bar{\boldsymbol{\beta}}^*) (G \boldsymbol{\gamma}_j \boldsymbol{\gamma}_j^T \sigma_{Yj}^{-2} G^T + V_{j,g}) + V_{j,g} \bar{\boldsymbol{\beta}} \bar{\boldsymbol{\beta}}^{*T} V_{j,g} \}$, I_L is an identity matrix of size $L \times L$.

Proof. We prove the asymptotic normality result first. Following the same argument as in the proof of Theorem 2, the objective function for MVMR-PACS (with light abuse of notation) can be simplified as

$$\Psi^{(n)}(\boldsymbol{\beta}) = \frac{1}{2}\boldsymbol{\beta}^T (\hat{\Pi}^T W \hat{\Pi} - V) \boldsymbol{\beta} - \hat{\boldsymbol{\Gamma}}^T W \hat{\Pi} \boldsymbol{\beta} + \lambda_n P(\boldsymbol{\beta})$$

Define $\mathbf{u} = r_n(\boldsymbol{\beta} - \boldsymbol{\beta}^*)$. Then, $\boldsymbol{\beta} = \boldsymbol{\beta}^* + \frac{\mathbf{u}}{r_n}$, where under the assumption $\mu_{n,\min}/\sqrt{p} \to \infty$, $r_n \to \infty$. Then, the objective function can be written as a function of \boldsymbol{u} as follows

$$\Psi^{(n)}(\boldsymbol{u}) = \frac{1}{2} (\boldsymbol{\beta}^* + \frac{\boldsymbol{u}}{r_n})^T (\hat{\Pi}^T W \hat{\Pi} - V) (\boldsymbol{\beta}^* + \frac{\boldsymbol{u}}{r_n}) - \hat{\Gamma}^T W \hat{\Pi} (\boldsymbol{\beta}^* + \frac{\boldsymbol{u}}{r_n}) + \lambda_n P (\boldsymbol{\beta}^* + \frac{\boldsymbol{u}}{r_n})$$

Let $\hat{\boldsymbol{u}}^{(n)} = \arg\min \Psi^{(n)}(\boldsymbol{u})$; then $\hat{\boldsymbol{\beta}}^{(n)} = \boldsymbol{\beta}^* + \frac{\hat{\boldsymbol{u}}^{(n)}}{r_n}$. Let $V^{(n)}(\boldsymbol{u}) = \Psi_n(\boldsymbol{u}) - \Psi_n(\boldsymbol{0})$. We know $\hat{\boldsymbol{u}}^{(n)}$ is also the minimizer of $V^{(n)}(\boldsymbol{u})$, where

$$V^{(n)}(\boldsymbol{u}) = \frac{1}{2r_n^2} \boldsymbol{u}^T (\hat{\Pi}^T W \hat{\Pi} - V) \boldsymbol{u} - \frac{1}{r_n} \boldsymbol{u}^T (\hat{\Pi}^T W \hat{\Gamma} - \hat{\Pi}^T W \hat{\Pi} \boldsymbol{\beta}^* + V \boldsymbol{\beta}^*)$$
$$+ \lambda_n \tilde{P}(u)$$

where

$$\tilde{P}(\boldsymbol{u}) = \sum_{k} \hat{w}_{k} \{ |\beta_{k}^{*} + \frac{u_{k}}{r_{n}}| - |\beta_{k}^{*}| \} + \sum_{1 \leq k < l \leq K} \hat{w}_{kl(-)} \{ |\beta_{k}^{*} - \beta_{l}^{*}| + \frac{u_{k} - u_{l}}{r_{n}}| - |\beta_{k}^{*} - \beta_{l}^{*}| \}$$

$$+ \sum_{1 \leq k < l \leq K} \hat{w}_{kl(+)} \{ |\beta_{k}^{*} + \beta_{l}^{*}| + \frac{u_{k} + u_{l}}{r_{n}}| - |\beta_{k}^{*} + \beta_{l}^{*}| \}$$

We now consider the limiting behavior of $\lambda_n \tilde{P}(\boldsymbol{u})$. We aim to show that $\lambda_n \tilde{P}(\boldsymbol{u})$ goes to 0 under correct sparsity and group structure and goes to infinity under the incorrect structure.

For all $k, l \in \{1, ..., K\}$, if $\beta_k^* \neq 0, \beta_l^* \neq 0$ and $\beta_k^* \neq \beta_l^*$, then $\hat{w}_k \xrightarrow{P} |\beta_k^*|^{-\tau}$, $\hat{w}_{kl(-)} \xrightarrow{P} c_{kl(-)} |\beta_k^* - \beta_l^*|^{-\tau}$ and $\hat{w}_{kl(+)} \xrightarrow{P} c_{kl(+)} |\beta_k^* + \beta_l^*|^{-\tau}$. Also, $r_n\{|\beta_k^* + \frac{u_k}{r_n}| - |\beta_k^*|\} \to u_k \text{sign}(\beta_k^*), r_n\{|\beta_k^* - \beta_l^* + \frac{u_k - u_l}{r_n}| - |\beta_k^* - \beta_l^*|\} \to (u_k - u_l) \text{sign}(\beta_k^* - \beta_l^*)$, and $r_n\{|\beta_k^* + \beta_l^* + \frac{u_k + u_l}{r_n}| - |\beta_k^* + \beta_l^*|\} \to (u_k + u_l) \text{sign}(\beta_k^* + \beta_l^*)$. By Slutsky's theorem, we have $\lambda_n \tilde{P}(\boldsymbol{u}) \xrightarrow{P} 0$ because $\lambda_n/r_n \to 0$.

If $\beta_k^* = 0$, then $r_n\{|\beta_k^* + \frac{u_k}{r_n}| - |\beta_k^*|\} = |u_k|$ and $\lambda_n \hat{w}_k\{|\beta_k^* + \frac{u_k}{r_n}| - |\beta_k^*|\} = \frac{\lambda_n}{r_n}|u_k|[\mathcal{V}_n]_{kk}^{-\frac{\tau}{2}}\{[\mathcal{V}_n]_{kk}^{-\frac{1}{2}}\tilde{\beta}_k\}^{-\tau} = \frac{\lambda_n}{r_n}|u_k|[\mathcal{V}_n]_{kk}^{-\frac{\tau}{2}}O_p(1)$, where the second equality is because $\tilde{\beta}_{\text{init}}$ is asymptotically normal, and hence $[\mathcal{V}_n]_{kk}^{-1}\tilde{\beta}_k \xrightarrow{D} N(0,1) = O_p(1)$, where \mathcal{V}_n is a consistent estimator of the asymptotic variance of $\tilde{\beta}_{\text{init}}$. Because the slowest rate at which the diagonal term of \mathcal{V}_n goes to 0 is r_n^{-2} by Lemma 8 in [11], we know $\frac{\lambda_n}{r_n}|u_k|[\mathcal{V}_n]_{kk}^{-\frac{\tau}{2}}O_p(1) = O_p(\lambda_n r_n^{\tau-1})|u_k|$. By the assumption that $\lambda_n r_n^{\tau-1} \to \infty$, we have $\lambda_n \hat{w}_k\{|\beta_k^* + \frac{u_k}{r_n}| - |\beta_k^*|\} \to \infty$ with probability tending one unless u_k goes to 0 sufficiently fast, faster than $\lambda_n r_n^{\tau-1}$.

Similarly, if $\beta_k^* = \beta_l^*$, then $r_n\{|\beta_k^* - \beta_l^* + \frac{u_k - u_l}{r_n}| - |\beta_k^* - \beta_l^*|\} = |u_k - u_l|$, and $\lambda_n \hat{w}_{kl(-)}\{|\beta_k^* - \beta_l^*| + \frac{u_k - u_l}{r_n}| - |\beta_k^* - \beta_l^*|\} = \lambda_n \hat{c}_{kl}|u_k - u_l|[\mathcal{V}_{n,kl}]^{-\frac{\tau}{2}}[\mathcal{V}_{n,kl}^{-\frac{1}{2}}(\tilde{\beta}_k - \tilde{\beta}_l)]^{-\tau}$, where $\mathcal{V}_{n,kl} = [\mathcal{V}_n]_{kk} + [\mathcal{V}_n]_{ll} - 2[\mathcal{V}_n]_{kl}$ denotes the consistent variance estimator of $\tilde{\beta}_k - \tilde{\beta}_l$. By the asymptotic normality of $\tilde{\beta}_{\text{init}}$, $\mathcal{V}_{n,kl}^{-\frac{1}{2}}(\tilde{\beta}_k - \tilde{\beta}_l) = O_p(1)$. Furthermore, because $\hat{c}_{kl(-)} \xrightarrow{P} c_{kl(-)}$, and the slowest rate at which $\tilde{\mathcal{V}}_n$ goes to 0 is r_n^{-2} , we have $\lambda_n \hat{w}_{kl(-)}\{|\beta_k^* - \beta_l^* + \frac{u_k - u_l}{r_n}| - |\beta_k^* - \beta_l^*|\} = \lambda_n \hat{c}_{kl}|u_k - u_l|[\mathcal{V}_{n,kl}]^{-\frac{\tau}{2}}[\mathcal{V}_{n,kl}^{-\frac{1}{2}}(\tilde{\beta}_k - \tilde{\beta}_l)]^{-\tau} = O_p(\lambda_n r_n^{\tau-1} c_{kl(-)}|u_k - u_l|)$. By the assumption that $\lambda_n r_n^{\tau-1} \to \infty$ and $0 < c_{kl(-)} < \infty$, we have $\lambda_n \hat{w}_{kl(-)}\{|\beta_k^* - \beta_l^* + \frac{u_k - u_l}{r_n}| - |\beta_k^* - \beta_l^*|\} \to \infty$ with probability tending one unless $u_k - u_l$ goes to 0 sufficiently fast, faster than $\lambda_n r_n^{\tau-1}$.

By the same argument, we can show that if $\beta_k^* = -\beta_l^*$, then $\lambda_n \hat{w}_{kl(+)}\{|\beta_k^* + \beta_l^* + \frac{u_k + u_l}{r_n}| - |\beta_k^* + \beta_l^*|\}$ $\to \infty$ with probability tending one unless $u_k + u_l$ goes to 0 sufficiently fast, faster than $\lambda_n r_n^{\tau-1}$. By proving via contradiction (similar to the arguments in the proof of Theorem 2), we can show that for those indices for which $\beta_k^* = 0$, the corresponding $\hat{u}_k \stackrel{P}{\to} 0$ at a rate faster than $\lambda_n r_n^{\tau-1}$; for those pairs of indices for which $\beta_k^* = \beta_l^*$, the corresponding $\hat{u}_k - \hat{u}_l \stackrel{P}{\to} 0$ at a rate faster than $\lambda_n r_n^{\tau-1}$; for those pairs of indices for which $\beta_k^* = -\beta_l^*$, the corresponding $\hat{u}_k + \hat{u}_l \stackrel{P}{\to} 0$ at a rate faster than $\lambda_n r_n^{\tau-1}$. In other words, $\hat{u}^{(n)}$ must have oracle structure with probability tending one as $n \to \infty$. Note that when u has the oracle structure, (i.e., for those indices for which $\beta_k^* = 0$, the corresponding $u_k = 0$; for those pairs of indices for which $\beta_k^* = \beta_l^*$, the corresponding $u_k = u_l$; for those pairs of indices for which $\beta_k^* = -\beta_l^*$, the corresponding $u_k = -u_l$), it is also true that $G^T C_g u = u$ by following almost the same argument as in the proof of Lemma 1. This implies that when n is large enough, $G^T C_g \hat{u}^{(n)} = \hat{u}^{(n)}$ holds with high probability.

As a result, when n is large enough, we can instead minimize $V^{(n)}(G^TC_g\boldsymbol{u})$ for \boldsymbol{u} . Note that

$$V^{(n)}(G^{T}C_{g}\boldsymbol{u}) = \frac{1}{r_{n}^{2}}\boldsymbol{u}^{T}C_{g}^{T}G(\hat{\Pi}^{T}W\hat{\Pi} - V)G^{T}C_{g}\boldsymbol{u} - \frac{1}{r_{n}}\boldsymbol{u}^{T}C_{g}^{T}G(\hat{\Pi}^{T}W\hat{\Gamma} - \hat{\Pi}^{T}W\hat{\Pi}\boldsymbol{\beta}^{*} + V\boldsymbol{\beta}^{*}) + \lambda_{n}\tilde{P}(G^{T}C_{g}\boldsymbol{u})$$

$$= \frac{1}{r_{n}^{2}}\boldsymbol{u}^{T}C_{g}^{T}G(\hat{\Pi}^{T}W\hat{\Pi} - V)G^{T}C_{g}\boldsymbol{u} - \frac{1}{r_{n}}\boldsymbol{u}^{T}C_{g}^{T}G(\hat{\Pi}^{T}W\hat{\Gamma} - \hat{\Pi}^{T}W\hat{\Pi}G^{T}C_{g}\boldsymbol{\beta}^{*} + VG^{T}C_{g}\boldsymbol{\beta}^{*})$$

$$+ \lambda_{n} \tilde{P}(G^{T}C_{g}\boldsymbol{u})$$

$$= \frac{1}{r_{n}^{2}}\boldsymbol{u}_{g}^{T}(\hat{\Pi}_{g}^{T}W\hat{\Pi}_{g} - V_{g})\boldsymbol{u}_{g} - \frac{1}{r_{n}}\boldsymbol{u}_{g}^{T}(\hat{\Pi}_{g}^{T}W\hat{\Gamma} - \hat{\Pi}_{g}^{T}W\hat{\Pi}_{g}C_{g}\boldsymbol{\beta}^{*} + V_{g}C_{g}\boldsymbol{\beta}^{*}) + \lambda_{n}\tilde{P}(G^{T}\boldsymbol{u}_{g})$$
(S9)

where we let $\mathbf{u}_g = C_g \mathbf{u} = (u_{g,1}, \dots, u_{g,L})^T$ be the transformed unknown parameters. (S9) is essentially the objective function after collapsing and droping the elements of $\hat{\gamma}_j$ according to the oracle structure.

Additionally, note that $\tilde{P}(G^T \boldsymbol{u}_g) = O_p(\lambda_n/r_n)(\sum_{k=1}^L u_{g,k} \operatorname{sign}(\bar{\beta}_k^*) + \sum_{1 \leq k < l \leq L} (u_{g,k} - u_{g,l}) \operatorname{sign}(\bar{\beta}_k^* - \bar{\beta}_l^*) + \sum_{1 \leq k < l \leq L} (u_{g,k} + u_{g,l}) \operatorname{sign}(\bar{\beta}_k^* + \bar{\beta}_l^*)) = O_p(\lambda_n/r_n) f(\boldsymbol{u}_g)$, where $f(\boldsymbol{u}_g) = \boldsymbol{a} + \boldsymbol{b}^T \boldsymbol{u}_g$ is a linear function in \boldsymbol{u}_g , where \boldsymbol{a} and \boldsymbol{b} are bounded constants. Therefore, when n is large enough, we only need to minimize

$$\frac{1}{r_n^2} \boldsymbol{u}_g^T (\hat{\Pi}_g^T W \hat{\Pi}_g - V_g) \boldsymbol{u}_g - \frac{1}{r_n} \boldsymbol{u}_g^T (\hat{\Pi}_g^T W \hat{\Gamma} - \hat{\Pi}_g^T W \hat{\Pi}_g C_g \boldsymbol{\beta}^* + V_g C_g \boldsymbol{\beta}^*) + O_p(\frac{\lambda_n}{r_n}) f(\boldsymbol{u}_g)$$

This objective is convex and the minimizer

$$\hat{\boldsymbol{u}}_{g}^{(n)} = r_{n}(\hat{\boldsymbol{\Pi}}_{g}^{T}W\hat{\boldsymbol{\Pi}}_{g} - V_{g})_{\mathcal{A}}^{-1}(\hat{\boldsymbol{\Pi}}_{g}^{T}W\hat{\boldsymbol{\Gamma}} - \hat{\boldsymbol{\Pi}}_{g}^{T}W\hat{\boldsymbol{\Pi}}_{g}C\boldsymbol{\beta}^{*} + V_{g}C\boldsymbol{\beta}^{*}) + O_{p}(\lambda_{n}/r_{n})(\hat{\boldsymbol{\Pi}}_{g}^{T}W\hat{\boldsymbol{\Pi}}_{g} - V_{g})^{-1}\boldsymbol{b}$$
Let $\hat{\boldsymbol{\beta}}_{g}^{(n)} = \bar{\boldsymbol{\beta}}^{*} + \boldsymbol{u}_{g}^{(n)}/r_{n}$. Then we have,
$$(\hat{\boldsymbol{\beta}}_{g}^{(n)} - \bar{\boldsymbol{\beta}}^{*}) = (\hat{\boldsymbol{\Pi}}_{g}^{T}W\hat{\boldsymbol{\Pi}}_{g} - V_{g})^{-1}(\hat{\boldsymbol{\Pi}}_{g}^{T}W\hat{\boldsymbol{\Gamma}} - \hat{\boldsymbol{\Pi}}_{g}^{T}W\hat{\boldsymbol{\Pi}}_{g}C\boldsymbol{\beta}^{*} + V_{g}C\boldsymbol{\beta}^{*}) + O_{p}(\lambda_{n})(\hat{\boldsymbol{\Pi}}_{g}^{T}W\hat{\boldsymbol{\Pi}}_{g} - V_{g})^{-1}\boldsymbol{b},$$
and

$$\mathbb{V}_{g}^{-\frac{1}{2}}(\Pi_{g}^{T}W\Pi_{g})(\hat{\boldsymbol{\beta}}_{g}^{(n)} - \bar{\boldsymbol{\beta}}^{*}) = \mathbb{V}_{g}^{-\frac{1}{2}}(\Pi_{g}^{T}W\Pi_{g})(\hat{\Pi}_{g}^{T}W\hat{\Pi}_{g} - V)^{-1}(\hat{\Pi}_{g}^{T}W\hat{\Gamma} - \hat{\Pi}_{g}^{T}W\hat{\Pi}_{g}C\boldsymbol{\beta}^{*} + V_{g}C\boldsymbol{\beta}^{*}) \\
+ O_{p}(\lambda_{n})\mathbb{V}_{g}^{-\frac{1}{2}}(\Pi_{g}^{T}W\Pi_{g})(\hat{\Pi}_{g}^{T}W\hat{\Pi}_{g} - V_{g})^{-1}\boldsymbol{b} \\
= \underbrace{\mathbb{V}_{g}^{-\frac{1}{2}}(\Pi_{g}^{T}W\Pi_{g})_{\mathcal{A}}(\hat{\Pi}_{g}^{T}W\hat{\Pi}_{g} - V_{g})^{-1}\mathbb{V}_{g}^{\frac{1}{2}}}_{A_{1}} \underbrace{\mathbb{V}_{g}^{-\frac{1}{2}}(\hat{\Pi}_{g}^{T}W\hat{\Gamma} - \hat{\Pi}_{g}^{T}W\hat{\Pi}_{g}C\boldsymbol{\beta}^{*} + V_{g}C\boldsymbol{\beta}^{*})}_{A_{2}} \\
+ O_{p}(\lambda_{n})\underbrace{\mathbb{V}_{g}^{-\frac{1}{2}}(\Pi_{g}^{T}W\Pi_{g})(\hat{\Pi}_{g}^{T}W\hat{\Pi}_{g} - V)^{-1}\mathbb{V}_{g}^{\frac{1}{2}}}_{\mathbf{y}}\mathbb{V}_{g}^{-\frac{1}{2}}\boldsymbol{b}$$

By the result S10 and Lemma 6 in [11], we know $A_1 \stackrel{P}{\to} I_L$ and $A_2 \stackrel{D}{\to} N(\mathbf{0}, I_L)$. Additionally, by Lemma 2 in the SRIVW paper, $\mathbb{V}_{\mathcal{A}}^{-\frac{1}{2}}$ goes to 0 at a rate at least $\sqrt{\mu_{n,\min} + p}$. Thus, the second term is of order $O_p(\lambda_n/\sqrt{\mu_{n,\min} + p}) = o_p(1)$ as $\lambda_n/r_n \to 0$. Then, by the Slutsky's theorem, we show the asymptotic normality of $\hat{\beta}_g^{(n)}$. Finally, note that $\hat{\beta}_g^{(n)} - \bar{\beta}^* = \mathbf{u}_g^{(n)}/r_n = C_g \mathbf{u}^{(n)}/r_n = C_g(\hat{\beta} - \boldsymbol{\beta}^*)$ by the definition of \mathbf{u}_g and \mathbf{u} . We complete the proof of asymptotic normality.

We now prove the consistency in risk factor selection and group identification. Note that the asymptotic normality result implies that for $\forall k \in \mathcal{B}$, $\mathbb{P}(k \in \mathcal{B}_n) \to 1$. It remains to show that $\forall k' \in \mathcal{B}^c$, $\mathbb{P}(k' \in \mathcal{B}_n) \to 0$. For $k' \in \mathcal{B}^c$, there are three possibility. First, there exists an index $m \in \{1, \ldots, K\}$ such that $\beta_m^* = 0$ but $\hat{\beta}_m \neq 0$. Second, there exists a pair of indices (m, l) for $m, l \in \{1, \ldots, K\}$ such that $\beta_m^* = \beta_l^*$ but $\hat{\beta}_m \neq \hat{\beta}_l$. Third, there exists a pair of indices (m, l) such that $\beta_m^* = -\beta_l^*$ but $\hat{\beta}_m \neq -\hat{\beta}_l$. In the following, we show by contradiction that these three

scenarios happen with probability tending 0.

For the first scenario, Since $\hat{\beta}_m \neq 0$, by the KKT conditions, we know $\hat{\beta}_m \neq 0$ satisfies

$$\left[(\hat{\Pi}^T W \hat{\Pi} - V) \hat{\boldsymbol{\beta}}^{(n)} - \hat{\Pi}^T W \hat{\boldsymbol{\Gamma}} \right]_m = \lambda_n \{ \hat{w}_m \operatorname{sign}(\hat{\beta}_m) + \sum_{1 \le j < m} \hat{w}_{jm(-)} \operatorname{sign}(\hat{\beta}_m - \hat{\beta}_j) + \sum_{m < k \le K} \hat{w}_{mk(-)} \operatorname{sign}(\hat{\beta}_k - \hat{\beta}_m) + \sum_{1 \le j < m} \hat{w}_{jm(+)} \operatorname{sign}(\hat{\beta}_m + \hat{\beta}_j) + \sum_{m < k \le K} \hat{w}_{mk(+)} \operatorname{sign}(\hat{\beta}_m + \hat{\beta}_k) \right]$$
(S10)

Following the same argument in the proof of Theorem 2, we can show that the left hand side is $O_p(\mu_{n,\max}/r_n)$ using the asymptotic normality result. Now we focus on the right hand side. Since $\beta_m = 0$, $[\mathcal{V}_n]_{mm}^{-\frac{1}{2}} \tilde{\beta}_m = O_p(1)$. Hence, $\hat{w}_m = [\mathcal{V}_n]_{mm}^{-\frac{\tau}{2}} ([\mathcal{V}_n]_{mm}^{-\frac{1}{2}} \tilde{\beta}_m)^{-\tau} = O_p(r_n^{\tau})$. Consider $\hat{w}_{jm(-)} = \hat{c}_{jm(-)}(|\tilde{\beta}_m - \tilde{\beta}_j|)^{-\tau}$ for j < m. If $\beta_j = 0$, then $\mathcal{V}_{n,jm}^{-\frac{1}{2}} (\tilde{\beta}_m - \tilde{\beta}_j) = O_p(1)$, where $\mathcal{V}_{n,jm} = [\mathcal{V}_n]_{kk} + [\mathcal{V}_n]_{kl} - 2[\mathcal{V}_n]_{kl}$ denotes the consistent variance estimator of $\tilde{\beta}_m - \tilde{\beta}_j$, and thus $\hat{w}_{jm(-)} = O_p(r_n^{\tau})$. If $\beta_j \neq 0$, then $|\tilde{\beta}_m - \tilde{\beta}_j| \xrightarrow{P} |\beta_j|$ and $\hat{w}_{jm(-)} = O_p(1)$. Hence, $\hat{w}_{jm(-)} = O_p(r_n^{\tau})$ for j < m. Similarly, we can argue that $\hat{w}_{mk(-)}$ for k > m, $\hat{w}_{jm(+)}$ for j < m, and $\hat{w}_{mk(+)}$ for k > m are all at most $O_p(r_n^{\tau})$. Therefore, the right hand side is at most $O_p(\lambda_n r_n^{\tau})$. By the assumption that $\lambda_n r_n^{\tau+1}/\mu_{n,\max} \to \infty$, we have a contradiction that (S10) cannot hold for large enough n.

For the second scenario, we only need to consider the case when $\beta_m = \beta_l \neq 0$, because the proof for the case when $\beta_m = \beta_l = 0$ follows directly from the proof in the first scenario. We again analyze the right hand side of (S10). For the first term, because $\beta_m^* \neq 0$, $|\tilde{\beta}_m| \stackrel{P}{\to} \beta_m^*$ and hence $\hat{w}_m = O_p(1)$. Then, consider $\hat{w}_{jm(-)} = \hat{c}_{jm(-)}(|\tilde{\beta}_m - \tilde{\beta}_j|)^{-\tau}$ for j < m and $\hat{w}_{mk(-)} = \hat{c}_{mk(-)}(|\tilde{\beta}_k - \tilde{\beta}_m|)^{-\tau}$ for m < k. For the indices l such that $\beta_l \neq \beta_m$, we know $|\tilde{\beta}_m - \tilde{\beta}_l| \stackrel{P}{\to} |\beta_m - \beta_l|$ and thus $\hat{w}_{lm} = O_p(1)$. For the indices l such that $\beta_l = \beta_m \neq 0$, we know $\mathcal{V}_{n,lm}^{-\frac{1}{2}}(\hat{\beta}_m - \hat{\beta}_l) = O_p(1)$ where $\mathcal{V}_{n,lm}$ denotes the consistent variance estimator of $\tilde{\beta}_m - \tilde{\beta}_l$. By the definition of this scenario, there exists at least one such an index l, and additionally, $\hat{\beta}_m \neq \hat{\beta}_l$. Therefore, we must have $\hat{w}_{lm(-)} \text{sign}(\hat{\beta}_m - \hat{\beta}_l) = O_p(r_n^{\tau})$. For the terms $\hat{w}_{jm(+)}$ and $\hat{w}_{mk(+)}$, following similar arguments, we know they are at most $O_p(r_n^{\tau})$. Therefore, the right hand side is $O_p(\lambda_n r_n^{\tau})$. Again, by the assumption that $\lambda_n r_n^{\tau+1}/\mu_{n,\max} \to \infty$, we have a contradiction that (S10) cannot hold for large enough n.

The proof for the third scenario mirrors the proof of the second scenario. We can follow similarly arguments to show for the pair of indices (m, l) such that $\beta_m^* = -\beta_l^* \neq 0$ but $\hat{\beta}_m \neq \hat{\beta}_l$, $\hat{w}_{ml(+)} \operatorname{sign}(\hat{\beta}_m + \hat{\beta}_l) = O_p(r_n^{\tau})$. Thus, the right hand side of (S10) is still $O_p(\lambda_n r_n^{\tau})$ and hence we still have a contradiction.